The Effects of PLX3397-induced Microglia Depletion on Huntington's Disease Progression in the R6/2 Mouse Model

Kaitlynn Perry
Integrated Program of Neuroscience
McGill University, Montreal
September 2021

A thesis submitted to McGill University in partial fulfillment of the requirements of the degree of Master of Neuroscience.

© Kaitlynn Perry 2021

Table of Contents

Author's Contributions

The main conceptual ideas and planning were outlined with advice from Dr. Abbas Sadikot and Dr. Vladimir Rymar. Experimental procedures and analysis were completed by myself under the supervision of Dr. Abbas Sadikot. The manuscript was written by myself with aid from Dr. Abbas Sadikot, and preliminary suggestions were also provided by my committee members, Dr. Timothy Kennedy and Dr. Luke Healy.

Acknowledgements

I would like to thank my supervisor, Dr. Abbas Sadikot, for providing me the opportunity to learn and grow as a scientist. To Dr. Sadikot along with my other committee members, Dr. Timothy Kennedy and Dr. Luke Healy, and my mentor, Dr. Edward Ruthazer: thank you for all of your support and guidance. Thank you Dr. Vladimir Rymar for all of your invaluable advice and for teaching me how to use the behavioural equipment. I would also like to thank Karl Asfour for providing me with the French translation of my abstract. Thank you members of the Cone Lab for the many enjoyable memories, insightful conversations, and advice both inside and outside of the lab. I would especially like to thank the Cone Lab, Strangers (my soccer teammates), friends, and my family for all of their support given to me these past three years.

Abstract

Huntington's Disease (HD) is a neurodegenerative disease caused by a polyglutamine mutation in the HTT gene, resulting in the mutant huntingtin protein (mhtt). Symptoms include cognitive and motor impairments that gradually worsen with age, and no curative treatment currently exists for HD. Increased inflammation and elevated microglia activation have been seen in many neurodegenerative diseases including HD, and correlative data has linked the level of microglia activation with HD progression. In addition to the many proposed hypotheses on how mhtt results in HD, mhtt-expressing microglia have also been shown to have altered functionality. Therefore, we wished to discern the impact microglia have in HD progression. Microglia ablation using PLX3397 – a CSF1R inhibitor – reduced symptoms in rodent models of other neurodegenerative diseases. Using a similar method, PLX3397 chow (290ppm or 600ppm) was provided to deplete microglia in the R6/2 model of HD. Their behavioural progression was monitored using the clasping test, inverted grid, open field, and elevated plus maze. Stereology was used to estimate the population of $Iba1^+$ microglia, $Nissl^+$ neurons, and parvalbumin interneurons in the striatum at 11.5 weeks. While R6/2 carriers appear to have increased microglia activation based on their subtype distribution, they also had lower rates of PLX3397-induced depletion compared to their wildtype littermates. The vehicle groups for R6/2 carriers and wildtype littermates followed the expected genotypic behavioural patterns, but R6/2 carriers showed no improvements in behaviour nor striatal neuron survival after microglia depletion. In accordance with associated literature, microglia do not have a prominent role in the behavioural symptoms nor striatal neurodegeneration of HD after symptom onset. However, as mhtt-related functional changes in microglia have been seen in presymptomatic HD carriers, further research is required to understand their impact on brain development and HD outcome.

Résumé

La maladie de Huntington (MH) est une maladie neurodégénérative causée par une mutation de polyglutamine sur le gène HTT, engendrant la protéine mutée huntingtin (mhtt). Les symptômes incluent des troubles cognitifs et moteurs qui se déteriorent graduellement avec l'âge. À l'heure actuelle, il n'existe toujours pas de traitements curatifs pour la MH. Des niveaux élevés d'inflammation et d'activation microgliale ont été observés dans plusieurs maladies neurodégératives dont la MH et des données corrélatives suggèrent un lien entre l'intensité de l'activation microgliale avec la progression de la MH. En plus des nombreuses hypothèses proposées sur le rôle de la mhtt dans le développement de la MH, certains ont démontré que la fonction des cellules microgliales exprimant la mhtt est altérée. Conséquemment, nous nous intéressons à l'impact des cellules microgliales sur la progression de la MH. L'ablation de cellules microgliales induite par PLX3397, un inhibiteur de CSF1R, permet de réduire les symptômes dans des modèles murins de d'autres maladies neurodégénératives. En utilisant une méthode similaire, nous avons incorporé PLX3397 (290 ppm ou 660 ppm) à la nourriture des souris afin de réduire le nombre de cellules microgliales dans le modèle R6/2 de la MH. Leur progression a été évaluée à l'aide de tests comportementaux tels que le test de dystonie, le test de suspension, le champ ouvert et le labyrinthe en croix surélevée. La stéréologie a été utilisé afin d'estimer les populations de cellules microgliales $Iba1^{+}$, de neurones $Nissl^{+}$, et d'interneurones à parvalbumine dans le striatum chez les souris agées de 11,5 semaines. Bien que la distribution des sous-types de cellules microgliales semble indiquer que les souris porteuses de la mutation R6/2 ont une activité microgliale augmentée, ces animaux ont également un plus faible taux de déplétion induite par PLX3397 que leurs confrères wildtypes. Les deux groupes de souris suivent un patron comportemental attendu; cependant, les souris mutantes R6/2 n'ont montré aucune amélioration dans leur comportement ni dans la survie des neurones striataux après la réduction des cellules microgliales. En accord avec la littérature, les cellules microgliales ne semblent donc pas avoir un rôle proéminent dans les symptômes comportementaux ni dans la neurodégénérescence striatale de la MH après l'émergence des premiers symptômes. Toutefois, considérant que les changements fonctionnels liés à la mhtt dans les cellules microgliales ont été observés chez des porteurs de la MH au stade présymptomatique, de plus amples recherches sont requises afin de comprendre leur impact sur le développement du cerveau et de la MH.

Chapter 1: The Role of Inflammation in Huntington's Disease and other neurodegenerative diseases and PLX3397-induced Microglia Depletion

Huntington's disease (HD) is an autosomal dominant neurodegenerative disorder caused by 36 or more CAG repeats in the huntingtin (HTT) gene found on chromosome 4, resulting in a mutant huntingtin protein (mhtt) (Roos 2010). The number of polyglutamine repeats correlates with the timing of the onset of symptoms, with more repeats indicative of an earlier onset (Roos 2010). The typical age of onset is between 30-50 years, but juvenile forms can occur in those younger than 20 (Roos 2010). Life expectancy is 17-20 years after symptom onset (Roos 2010). Symptoms typically progress from neuropsychiatric features, such as depression, apathy, and memory loss, to motor impairments, such as involuntary movement and akinesia (Roos 2010). The motor symptoms increase in severity over the duration of the disease until complete dependency in daily life is required (Roos 2010). There is currently no cure for HD, and treatment is aimed at alleviating the symptoms (Roos 2010).

1.1 Mutant Huntingtin Toxicity and Proposed Mechanisms of Cellular Loss in HD

Wild-type huntingtin (htt) is ubiquitously expressed in the entire body and is involved with intracellular transport, synaptic functioning (such as synaptic vesicle recycling and receptor endocytosis), gene expression, and cellular metabolism (Li and Li 2004, Roos 2010, Morigaki and Goto 2017). However, with the addition of polyglutamine repeats, mhtt gains a toxic role. The expression of N-terminal mhtt fragments induced apoptosis in striatal neuron cultures, which was prevented by anti-apoptotic compounds and neurotrophic factors (Saudou, Finkbeiner et al. 1998). Additionally, mhtt increases susceptibility to apoptotic stress as seen in lymphoblasts from HD patients (Sawa, Wiegand et al. 1999). The toxic role of the mutation is believed to originate from both the loss and gain of functions. The mutation impacts normal interactions with htt-binding partners, which includes important transcription factors and repressors (Sawa, Tomoda et al. 2003). For example, mhtt loses its ability to retain brain-derived neurotrophic factor (BDNF) repressor in the cytoplasm, leading to decreased BDNF transcription and

transport – which are important for striatal neurons' differentiation and survival (Li and Li 2004, Zuccato and Cattaneo 2007, Morigaki and Goto 2017). However, endogenous htt does not ameliorate HD pathology caused by mhtt (Li and Li 2004). Furthermore, recruitment of htt into the aggregates formed by mhtt may lower the availability of the endogenous protein (Masnata, Sciacca et al. 2019). The presence of other polyglutamine diseases with neurological deficits, such as spinocerebellar ataxia (SCA), indicates that there may also be a toxic function gained from the polyglutamine repeats themselves (Sawa, Tomoda et al. 2003).

Neurodegeneration in HD mainly affects the striatum, which includes the caudate nucleus and putamen (Báez-Mendoza and Schultz 2013). It is important for processing motor and goal-orientated behaviour and facilitating voluntary movement, while also being involved with reward processing and decision-making (Báez-Mendoza and Schultz 2013). Medium spiny neurons (MSNs) make up 95% of neurons in the human striatum and 90% in the rodent striatum (Morigaki and Goto 2017). Progressive neuronal loss – primarily of MSNs, parvalbumin interneurons, and calretinin interneurons – in the striatum explains many of the symptoms present in HD patients (Imarisio, Carmichael et al. 2008, Reiner, Shelby et al. 2013, Samadi, Boutet et al. 2013, Morigaki and Goto 2017, Paldino, Cardinale et al. 2017). There are a number of hypotheses regarding the selective vulnerability of MSNs in HD. It has been hypothesized that striatal MSNs are more vulnerable to neurodegeneration due to increased susceptibility to glutamate-induced excitotoxicity due to specialized NMDA receptors on the striatal MSNs (Sawa, Tomoda et al. 2003, Ramaswamy, McBride et al. 2007). Another hypothesis proposed that MSNs have increased susceptibility to mitochondria dysfunction, leading to oxidative stress (Sawa, Tomoda et al. 2003, Ramaswamy, McBride et al. 2007). Furthermore, loss of neurotrophic support for MSNs due to altered transcription has also been suggested (Sari 2011). Given the complex role of mhtt, all of these dysregulated processes may be working in concert to give MSNs their vulnerability to degeneration.

1.2 Role of Inflammation in Neurodegenerative Diseases

There is extensive literature on immune activation in neurodegenerative diseases. Increased pro-inflammatory cytokines and increased microglial activation is seen in multiple neurodegenerative diseases, including HD, SCA, Alzheimer's Disease (AD), Parkinson's Disease (PD), and

Multiple Sclerosis (MS) (Amor, Peferoen et al. 2014, Stephenson, Nutma et al. 2018). Although acute immune response in the CNS has been shown to be beneficial for tissue repair and restoring homeostasis, exaggerated and prolonged immune responses can be damaging (Amor, Peferoen et al. 2014). This may be due to neurons facing collateral damage due to an immune-mediated attack on a nearby cell or the presence of pro-inflammatory factors (Amor, Peferoen et al. 2014). In addition, damaged neurons release chemokines to attract immune cells, and neuronal loss decreases inhibitory signalling to control pro-inflammatory cytokine and neurotoxic molecule production, both of which could perpetuate the damage (Amor, Peferoen et al. 2014). The impact of the immune system on neurodegenerative diseases is apparent, as peripheral inflammation has been shown to exacerbate experimental AD, PD, MS, stroke, and prion disease (Perry 2010). Transgenic mice develop less severe neurodegeneration in pathogen-free conditions (Capsoni, Carucci et al. 2012). Also, there is a lower prevalence of AD in regular non-steroidal anti-inflammatory drug users, suggesting a role of inflammation in the development of the disease (Jaturapatporn, Isaac et al. 2012). Furthermore, there is increased inflammation, decreased ability to repair damage, and decreased immune response with age, which is a large risk factor for many neurodegenerative diseases (Amor, Peferoen et al. 2014). For example, the production of AGE, which after activating the RAGE receptor leads to pro-inflammatory cytokines and free radicals, is accelerated in MS, AD, and PD (Harris and Amor 2011, Amor, Peferoen et al. 2014). In aged mice, there is increased dysmorphic microglia which have higher levels of activation and overreact to stimulus with an exaggerated cytokine release response (Shimada and Hasegawa-Ishii 2011).

1.3 Microglia and their Role in Huntington's Disease

As microglia are the resident CNS immune cell, they are of marked interest for their role in neurodegenerative diseases. They originate from yolk sac macrophages and contribute to 5-20% of the total glial population (Barres, Freeman et al. 2015, Kawabori and Yenari 2015). They are long-lived (up to 4.2 years in humans) and self-renew to maintain their population (Hashimoto, Chow et al. 2013, Barres, Freeman et al. 2015, Réu, Khosravi et al. 2017). In the healthy brain, they are involved in nervous system development: assisting through facilitating programmed cell death, synaptic pruning and maturation, and secreting factors that promote neuronal survival and

proliferation (Barres, Freeman et al. 2015, Bilimoria and Stevens 2015). Their regulatory role persists into adulthood: while in their resting state, their motile processes survey the entire brain parenchyma within hours (Nimmerjahn, Kirchhoff et al. 2005, Barres, Freeman et al. 2015). They engulf dead or dying cells and debris during brain development and after injury (Bilimoria and Stevens 2015). However, after injury, whether from infection, inflammation, ischemia, or neurodegeneration, the microglia become activated, which changes their morphology from ramified to amoeboid – morphologically similar to circulating macrophages (Brown and Neher 2014, Kawabori and Yenari 2015). The activated microglia migrate to the source of the injury and proliferate (Webster, Hokari et al. 2013, Kawabori and Yenari 2015). However, activated microglia can either help repair the damage or exacerbate the problem, depending on the duration of the injury. Acute injury is believed to lead to a protective phenotype that secretes factors that are anti-inflammatory and aid in wound repair, such as transforming growth factor beta (TGFβ) and IL10 (Kawabori and Yenari 2015). After continuous activation from prolonged injury, the microglia are believed to take a pro-inflammatory phenotype, which increases inflammation and induces apoptosis through release of TNFα, nitric oxide (NO), IL6, and IL1β (Kawabori and Yenari 2015).

High levels of microglial activation are involved in the progression of neurodegenerative diseases, including AD, PD, and HD (Schwab, Klegeris et al. 2010, Ellrichmann, Reick et al. 2013). Chronic neuroinflammation often coincides with activated microglia in those disease states (Lull and Block 2010). Even in presymptomatic HD gene carriers, there are increased microglial activation and density (Myers, Vonsattel et al. 1991, Politis, Lahiri et al. 2015). Furthermore, the severity of HD pathology correlates with the density of activated microglia (Sapp, Kegel et al. 2001, Pavese, Gerhard et al. 2006, Yang, Yang et al. 2017). Microglia containing mhtt have shown higher expression of pro-inflammatory factors, reduced migration to chemotactic stimulus, and increased ability to induce neuronal death in cell cultures and in the presence of inflammation *in vivo* (Kwan, Träger et al. 2012, Crotti, Benner et al. 2014). Thus, microglia may exacerbate neurodegeneration in HD, as continued production of pro-inflammatory factors can damage cells and the blood-brain barrier (da Fonseca, Matias et al. 2014). Furthermore, in response to brain injury caused by neuroinflammation, AD, or brain ischemia, microglia can phagocytose stressed-but-viable cells – including neurons – due to stressors inducing eat-me signals on them (Brown and Neher 2014). Regulating microglia in HD

may alleviate the disease progression, as studies have shown that reducing microglia activation via pharmaceutical treatment has been neuroprotective in models of neurodegenerative diseases (Li, Yuan et al. 2013, Morsali, Bechtold et al. 2013, Amor, Peferoen et al. 2014).

1.4 Animal Models of HD

Animal models of HD are divided into toxin-induced models and genetic models. The toxins commonly used are quinolinic acid (QA; a NMDAR agonist) and 3-nitropropionic acid (3-NP; a mitochondria inhibitor) (Ramaswamy, McBride et al. 2007). Both have been used in rodents and non-human primates to cause acute cell death within the striatum, each acting through a different hypothesized method of cell death in HD (Ramaswamy, McBride et al. 2007). While QA is injected directly into the striatum, and thus can be used for unilateral degeneration, 3-NP is given systemically, thus causing bilateral degeneration (Ramaswamy, McBride et al. 2007). QA models develop symptoms similar to early HD, while 3-NP models can mimic early or late HD depending on the dosage (Ramaswamy, McBride et al. 2007). Although the toxins act through the mechanisms hypothesized to cause degeneration in HD, the models do not develop mhtt and thus cannot mimic other aspects of HD unrelated to striatal degeneration. Furthermore, because of the instantaneous nature of the toxin, the progressive pathological aspects seen in the disease cannot be studied. Thus, when the gene causing HD was discovered, transgenic models (R6/2, R6/1, N171-82Q, YAC) and knock-in models (HdhQ111, CAG150) were created. While the knock-in models are the closest genetically to replicating HD, their pathology has not been able to mimic the disease as well as the transgenic models (Ramaswamy, McBride et al. 2007). From the transgenic models, the most commonly used is the R6/2. The R6/2, R6/1, and N171-82Q models contain a mhtt fragment, while the YAC models contain the full gene (Ramaswamy, McBride et al. 2007). The transgene in the R6/2, R6/1, and YAC models is under the control of the human htt promoter, while the N171-82Q model uses the mouse prion promoter to express mhtt in neurons and not glia (Ramaswamy, McBride et al. 2007). Whereas the other transgenic models aforementioned have a prolonged disease progression which mimics adult HD, R6/2 mice have a fast progression of symptoms which extensive research has shown reproduces the motor and neuropathological symptoms of juvenile HD (Ramaswamy, McBride et al. 2007).

The R6/2 mouse model of HD contains exon 1 of the human HTT gene containing 120-150 CAG repeats, mimicking a faster progressing juvenile phenotype (Mangiarini, Sathasivam et al. 1996, Ferrante 2009, Savage, St-Pierre et al. 2020). They generally live until 13 weeks (Li, Popovic et al. 2005, Ferrante 2009, Samadi, Boutet et al. 2013). They show decreased anxiety-like behaviour and involuntary clasping at 4 weeks, prior to most of their motor symptom onset (Li, Popovic et al. 2005, Cowin, Bui et al. 2011, Samadi, Boutet et al. 2013). At around 8 weeks of age, the mice develop motor coordination impairments, grip strength reduction, muscle atrophy, and weight loss – all which worsens with age (Sathasivam, Hobbs et al. 1999, Li, Popovic et al. 2005, Ferrante 2009, Schwab, Klegeris et al. 2010, Cowin, Bui et al. 2011, Samadi, Boutet et al. 2013). Hyperactivity seen at 3 weeks of age progressively declines to hypoactivity around 7-8 weeks (Li, Popovic et al. 2005, Samadi, Boutet et al. 2013). In later stages of the disease, the motor impairments make eating difficult, which mimics the human pathology (van der Burg, Bacos et al. 2008). The mice have notable striatal volume decreases starting at 6 weeks, followed by striatal neuron atrophy at 9 weeks and striatal neuron loss at 11 weeks (Cowin, Bui et al. 2011, Samadi, Boutet et al. 2013, Dodds, Chen et al. 2014). There are also significantly less parvalbumin interneurons in the striatum after 13 weeks (Reiner, Shelby et al. 2013, Paldino, Cardinale et al. 2017). The mice show similar changes to its cellular functions compared to HD patients – including altered intracellular trafficking, transcriptional regulation, and metabolism – indicating the disease in the R6/2 mouse model functions through similar mechanisms as the human pathogenesis (Ferrante 2009). Inflammatory factors – including IL1β, IL6, IL10, and IL12 – in the serum and activated microglia in the R6/2 striatum are also heightened (Björkqvist, Wild et al. 2008, Schwab, Klegeris et al. 2010, Yang, Yang et al. 2017).

1.5 Biological action of PLX3397

Pexidartinib (PLX3397) is a polar and non-charged molecule that is used to eliminate tumor-associated macrophages and microglia (Elmore, Lee et al. 2015). It can bypass the blood-brain barrier without active transport, and inhibits colony stimulating factor 1 receptor (CSF1R), KIT proto-oncogene receptor tyrosine kinase (cKIT), and fms-like tyrosine kinase 3 (FLT3) (El-Gamal, Al-Ameen et al. 2018). All three members of the type III receptor tyrosine kinase family are important for cell proliferation, differentiation, and survival (Zhang and Fedoroff 1998,

DeBoy, Rus et al. 2010, Achkova and Maher 2016, El-Gamal, Al-Ameen et al. 2018, Li and Barres 2018).

CSF1R is the main target of PLX3397. It is specifically expressed in myeloid lineage cells, including microglia and macrophages, and is evolutionarily highly conserved (Elmore, Lee et al. 2015, Achkova and Maher 2016, El-Gamal, Al-Ameen et al. 2018). PLX3397 prevents CSF1R activation by binding the autoinhibited state of CSF1R (Tap, Wainberg et al. 2015, El-Gamal, Al-Ameen et al. 2018). CSF1R KO or $CSF1R^{null/null}$ mouse models have reduced levels of tissue macrophages, including microglia (Barres, Freeman et al. 2015). However, PLX3397 treatment has not been found to deplete healthy macrophages or other myeloid-lineage cells expressing CSF1R (Mok, Koya et al. 2014, Li, Li et al. 2017). cKIT is found on microglia, astrocytes, and hematopoietic progenitors, while FLT3 is present on hematopoietic cells, dendritic cells, and microglia (Zhang and Fedoroff 1997, DeBoy, Rus et al. 2010, Perdiguero, Klapproth et al. 2015). Both appear important for microglia function. cKIT activation is important for microglia survival and maintaining microglia in a resting state, and is upregulated in activated microglia after injury (Zhang and Fedoroff 1998, Zhang and Fedoroff 1999). FLT3 is involved with the pro-inflammatory response of activated microglia, as blockage of FLT3 signaling *in vitro* in activated mouse microglia dampened the pro-inflammatory response in a dose-dependent manner (DeBoy, Rus et al. 2010).

Table 1. Overview of PLX3397-induced microglia depletion in healthy mice and mouse models of neurodegenerative diseases.

Model	PLX3397 Dosage	Duration	Method of Detection	Microglia Depletion	Reference
C57BL/6/129 mix	290ppm chow	21 days	$Iba1^+$ IHC	>99%	Elmore, Najafi et al. (2014)
CX3CR1-$GFP^{+/-}$	290ppm chow	7 days	GFP^+ Flow Cytometry	>90%	
5xfAD	290ppm chow	3 months	$Iba1^+$ IF	~70-80% & >99% of area fraction in WT & 5xfAD	Sosna, Philipp et al. (2018)
5xfAD	290ppm chow	28 days	$Iba1^+$ IF	~80% in WT & 5xfAD	Spangenberg, Lee et al. (2016)
ATXN1[82Q]	~200 mg/kg body weight	2 months	$Iba1^+$ IF	Density: 82% in WT, 69% in ATXN1[82Q]	Qu, Johnson et al. (2017)
Tg4510	290ppm chow	3 months	$Iba1^+$ IHC (& Stereology)	Density: 30% in WT & Tg4510	Bennett, Bryant et al. (2018)

IHC = immunohistochemistry, IF = immunofluorescence

1.6 Effects of PLX3397-induced Microglia Depletion

PLX3397 has been used *in vitro* and *in vivo* (Elmore, Najafi et al. 2014). The most common route of application *in vivo* is through the diet, at a dosage of 290ppm (Elmore, Najafi et al. 2014, Elmore, Lee et al. 2015, Li, Li et al. 2017, Li, Li et al. 2017). The compound can be tolerated at higher doses, with the highest dose tested (1160ppm chow) having no noted ill effects (Elmore, Najafi et al. 2014). After 21 days of PLX3397 chow at 290ppm, C57BL/6/129 mice showed a 99% reduction of microglia, with a majority of the depletion (70-90%) within the first 7 days (Elmore, Najafi et al. 2014, Elmore, Lee et al. 2015, Rice, Spangenberg et al. 2015). Reduction appears to be due to apoptosis of microglia, not deactivation (Elmore, Najafi et al. 2014). However, the remaining $Iba1^+$ cells repopulate the brain after 3 days of halting the treatment, so PLX3397 must be continually administered for sustained microglial ablation (Elmore, Najafi et al. 2014, Elmore, Lee et al. 2015, Huang, Xu et al. 2018). Studies in healthy mice have found no cognitive nor behavioural differences between adult mice taking PLX3397 or vehicle, nor were there any other notable side effects, even after 3 months of continuous treatment (Elmore, Najafi et al. 2014, Rice, Spangenberg et al. 2015, Sosna, Philipp et al. 2018). Additionally, there were no cognitive, behavioural, nor motor changes after the mice were taken off PLX3397 and the microglia re-populated (Elmore, Lee et al. 2015). Currently, PLX3397 is in phase 3 of clinical trials for cancer treatment (Daiichi Sankyo 2015).

Microglia depletion has been proven to partially reverse pathophysiology in various animal models of neurodegenerative diseases. Microglial ablation (~80%) using PLX3397 chow at 290ppm in the 5xfAD mouse model of AD led to improved contextual memory, reduced expression of pro-inflammatory genes, and prevented neuronal loss after 1 month of treatment, and decreased proteins that are hallmark to the disease after 3 months of treatment (Spangenberg, Lee et al. 2016, Sosna, Philipp et al. 2018). Furthermore, 21 days of PLX3397 treatment via gavage at 40mg/kg/day in mice depleted 90% of their microglia and reduced their inflammatory proteins (IL1α, IL1β, IL6, IFNγ, GM-CSF) after intracerebral hemorrhage without altering their baseline expression prior to injury (Li, Li et al. 2017). PLX3397 treatment for 2 months in a SCA type 1 mouse model, ATXN1[82Q], reduced microglia density by 69%, improved motor coordination, and decreased TNFα expression (Qu, Johnson et al. 2017). PLX3397 decreased Iba1 protein levels by 72%, improved depressive-like behaviour and motor symptoms, and

partially recovered the dopamine neurotransmission in the 6-OHDA rat model of PD (Oh, Ahn et al. 2020). In a recent study in the R6/2 model, PLX3397 chow at 275ppm for 5 weeks resulted in a large decrease in microglia density in both carriers and wildtype littermates, and treatment improved forepaw grip strength and novel object recognition deficits, rescued dorsal striatum volume loss, and reduced soluble mhtt and their aggregates in carrier mice (Crapser, Ochaba et al. 2020).

1.7 Hypothesis and Experimental Plan

Neuroinflammation and increased microglial activation are seen in many neurodegenerative diseases, including HD and the R6/2 mouse model. As microglia depletion in rodent models of other neurodegenerative diseases has alleviated some of their symptoms, the depletion of microglia in the R6/2 model may reveal the role microglia plays in HD progression.

We hypothesized that continuous PLX3397 administration through chow at 290ppm *ad libitum* for 3 or more weeks would cause substantial microglia reduction in R6/2 mice. Furthermore, we hypothesized that significant microglia depletion would slow or halt HD progression in the R6/2 model.

To address these questions, microglia in R6/2 mice were ablated using PLX3397, and their disease progression was assessed using behavioural tests (clasping, inverted grid, open field, elevated plus maze). The total microglia numbers, proportion of microglia at different activation stages, total neuron numbers, and parvalbumin interneuron numbers were quantified using immunohistochemistry and stereology, to determine the extent of PLX3397-induced microglia depletion, microglia activation, and neurodegeneration in the striatum.

Chapter 2: The Effects of PLX3397-induced Microglia Depletion on Huntington's Disease Progression in the R6/2 Mouse Model

2.1 Abstract

Huntington's Disease (HD) is a neurodegenerative disease caused by a polyglutamine mutation in the HTT gene, resulting in the mutant huntingtin protein (mhtt). Symptoms include cognitive and motor impairments that gradually worsen with age, and no curative treatment currently exists for HD. Increased inflammation and microglia activation is present in many neurodegenerative diseases including HD, and chronically active microglia have been shown to correlate with HD progression. Furthermore, mhtt-expressing microglia have shown abnormalities in their regular functions. In other neurodegenerative diseases with similar neuroinflammatory profiles, PLX3397-induced microglia depletion was able to reduce symptoms in their rodent models. To assess if microglia play a similar detrimental in HD symptomology, we used PLX3397 chow (290ppm or 600ppm) to deplete microglia in the R6/2 model of HD and monitored their behavioural progression using the clasping test, inverted grid, open field, and elevated plus maze. The populations of $Iba1^+$ microglia, $Nissl^+$ neurons, and parvalbumin interneurons in the striatum at 11.5 weeks were estimated using stereology. Increased microglia activation was detected in R6/2 carriers based on their subtype distribution compared to their wildtype littermates. PLX3397 treatment at 290ppm resulted in 31% microglia depletion in R6/2 carriers, and treatment at 600ppm revealed that R6/2 carriers were less responsive to PLX3397-induced microglia depletion (57%) compared to their wildtype littermates (91%). While the controls followed their expected genotypic behavioural patterns, there were no improvements in R6/2 carriers due to microglia depletion at either dose. Striatal neuron loss was not improved by low-dose treatment, however there was a non-significant trend for increased parvalbumin interneuron survival. In summary, our findings indicate that microglia do not play a prominent role in HD symptomology nor neuropathology in the R6/2 model after symptom onset. This is in agreeance with other literature on HD rodent models. Although $mhtt^+$ microglia do not have clear behavioural implications after symptom onset, further research is required to determine the role of $mhtt^+$ microglia during brain development and maturation on HD outcome.

2.2 Introduction

The purpose of this study is to look at the extent microglia play in the progression of Huntington's Disease (HD). HD is an autosomal dominant neurodegenerative disorder caused by a mutation in the huntingtin gene (HTT) found on chromosome 4, resulting in mutant huntingtin protein (mhtt) (Roos 2010). HD typically presents when there are 36 or more CAG repeats in HTT, with more repeats correlating with an earlier onset of symptoms (Roos 2010). Therefore while the typical age of onset is between 30-50 years, juvenile forms can present in those younger than 20 (Roos 2010). Symptoms typically progress from neuropsychiatric features, such as depression, apathy, and memory loss, to motor impairments, such as involuntary movement and akinesia (Roos 2010). Motor symptoms increase in severity over the duration of the disease until complete dependency in daily life is required (Roos 2010). Life expectancy is 17-20 years after symptom onset (Roos 2010). Due to the lack of a cure for HD, treatment is currently aimed at alleviating symptoms (Roos 2010).

Wild-type huntingtin (htt) is ubiquitously expressed in the entire body and is involved with intracellular transport, synaptic functioning (such as synaptic vesicle recycling and receptor endocytosis), gene expression, and cellular metabolism (Li and Li 2004, Roos 2010, Morigaki and Goto 2017). The mutation is believed to cause both the loss and gain of functions. One function mhtt loses is its ability to retain brain-derived neurotrophic factor (BDNF) repressor in the cytoplasm; this leads to reduced BDNF transcription and transport, which are important for striatal neurons' differentiation and survival (Li and Li 2004, Zuccato and Cattaneo 2007, Morigaki and Goto 2017). However, the cellular changes due to mhtt cannot be solely due to loss of function as the presence of endogenous htt does not ameliorate HD pathology in HD mouse models (Li and Li 2004). Post-mortem brains of patients with HD revealed progressive neuronal loss – primarily of medium spiny neurons, parvalbumin interneurons, and calretinin interneurons in the striatum – and brain volume loss (Imarisio, Carmichael et al. 2008, Reiner, Shelby et al. 2013, Samadi, Boutet et al. 2013, Morigaki and Goto 2017, Paldino, Cardinale et al. 2017). Degeneration also occurs in the deep layers of the cerebral cortex, and in later stages, the hypothalamus and hippocampus (Li and Li 2004). Affected regions have increased inflammation, which is common for most neurodegenerative diseases; in particular, the plasma and striatum of HD patients show elevated levels of pro-inflammatory cytokines, including

interleukin 6 (IL6), IL8, and tumor necrosis factor alpha (TNFα) (Schwab, Klegeris et al. 2010, Nayak, Ansar et al. 2011, Yang, Yang et al. 2017).

The R6/2 mouse model of HD has exon 1 of the human HTT gene containing 120-150 CAG repeats (Mangiarini, Sathasivam et al. 1996, Ferrante 2009, Savage, St-Pierre et al. 2020). It mimics that of a faster progressing juvenile phenotype, with a lifespan of approximately 13 weeks (Mangiarini, Sathasivam et al. 1996, Li, Popovic et al. 2005, Ferrante 2009, Samadi, Boutet et al. 2013). At 4 weeks, which is prior to most of their motor symptom onset, they show decreased anxiety-like behaviour and involuntary clasping (Li, Popovic et al. 2005, Cowin, Bui et al. 2011, Samadi, Boutet et al. 2013). Hyperactivity seen at 3 weeks of age progressively declines to hypoactivity around 7-8 weeks (Li, Popovic et al. 2005, Samadi, Boutet et al. 2013). At around 8 weeks, they develop motor coordination impairments, grip strength reduction, muscle atrophy, and weight loss – all of which worsens with age (Sathasivam, Hobbs et al. 1999, Li, Popovic et al. 2005, Ferrante 2009, Schwab, Klegeris et al. 2010, Cowin, Bui et al. 2011, Samadi, Boutet et al. 2013). In later stages of the disease, the motor impairments make eating difficult, which mimics the human pathology (van der Burg, Bacos et al. 2008). R6/2 mice have a rapid progressive deterioration of their striatum: starting with notable striatal volume decreases at 6 weeks, followed by striatal neuron atrophy at 9 weeks and striatal neuron loss at 11 weeks, and then significant loss of parvalbumin interneurons at 13 weeks (Cowin, Bui et al. 2011, Reiner, Shelby et al. 2013, Samadi, Boutet et al. 2013, Dodds, Chen et al. 2014, Paldino, Cardinale et al. 2017). The loss of parvalbumin interneurons appear to contribute to dystonia, as the severity of parvalbumin interneuron loss correlates with the severity of dystonia in both HD patients and rodent models (Reiner, Shelby et al. 2013). Furthermore, R6/2 mice share similar abnormalities in their cellular functions with HD patients including alterations in their intracellular trafficking, transcriptional regulation, and metabolism, which indicates the disease in the R6/2 mouse model functions through similar mechanisms as the human pathogenesis (Ferrante 2009). Inflammatory factors – including IL1β, IL6, IL10, and TNFα – are also increased in the R6/2 striatum, possibly from activated microglia (Schwab, Klegeris et al. 2010, Hsiao, Chiu et al. 2014, Yang, Yang et al. 2017).

Microglia are brain-resident macrophages which originate from yolk sac macrophages (Barres, Freeman et al. 2015). Their population contributes to 5-20% of the total glial population, which the microglia maintain through their self-renewal and long lifespans (up to 4.2 years in

humans) (Hashimoto, Chow et al. 2013, Barres, Freeman et al. 2015, Kawabori and Yenari 2015, Réu, Khosravi et al. 2017). In the healthy brain, microglia have a plethora of roles to ensure normal nervous system development such as facilitating programmed cell death, synaptic pruning and maturation, and secreting factors that promote neuronal survival and proliferation (Barres, Freeman et al. 2015, Bilimoria and Stevens 2015). Their regulatory role persists into adulthood: microglia in their resting state survey the entire brain parenchyma within hours using their motile processes (Nimmerjahn, Kirchhoff et al. 2005, Barres, Freeman et al. 2015). They phagocytose dead or dying cells and debris during brain development and after injury (Bilimoria and Stevens 2015). However, after injury, whether from infection, inflammation, ischemia, or neurodegeneration, the microglia become activated (Kawabori and Yenari 2015). This alters their morphology from ramified to amoeboid – morphologically similar to circulating macrophages – so that the activated microglia can migrate to the source of the injury and proliferate (Webster, Hokari et al. 2013, Brown and Neher 2014, Kawabori and Yenari 2015). However, the duration of the injury impacts whether activated microglia help repair or exacerbate the damage. A protective phenotype that secretes factors that are anti-inflammatory and aid in wound repair, such as transforming growth factor beta (TGFβ) and IL10, is believed to emerge from acute injury (Kawabori and Yenari 2015). Conversely, continuous activation from prolonged injury is believed to transform microglia into a pro-inflammatory phenotype, which increases inflammation and induces apoptosis through the release of TNFα, nitric oxide (NO), IL6, and IL1β (Kawabori and Yenari 2015).

High levels of microglial activation are involved in the progression of neurodegenerative diseases, including Alzheimer's Disease, Parkinson's Disease, and HD (Schwab, Klegeris et al. 2010). Furthermore, chronic neuroinflammation often coincides with activated microglia in these disease states (Lull and Block 2010). This can be detrimental as the continued production of pro-inflammatory factors can damage cells and the blood-brain barrier (da Fonseca, Matias et al. 2014). In cases of brain injury, such as neuroinflammation, Alzheimer's Disease, and brain ischemia, microglia can also phagocytose live cells – including neurons – due to stressors inducing eat-me signals on stressed-but-viable cells (Brown and Neher 2014). The increased presence of activated microglia in the brain applies not only to HD patients, but the R6/2 mouse model as well (Simmons, Casale et al. 2007, Ellrichmann, Reick et al. 2013). Furthermore, increased microglia activation and density is even present in presymptomatic HD carriers

(Myers, Vonsattel et al. 1991, Politis, Lahiri et al. 2015). Microglia density appears to be of grave importance for HD as there is a correlation between the density of activated microglia and the severity of HD pathology (Sapp, Kegel et al. 2001, Pavese, Gerhard et al. 2006, Yang, Yang et al. 2017). Additionally, mhtt impacts normal microglia functionality. Microglia expressing mhtt have higher expression of pro-inflammatory factors, reduced migration to chemotactic stimulus, and increased ability to induce neuronal death in the presence of inflammation (Kwan, Träger et al. 2012, Crotti, Benner et al. 2014). However, it is unclear whether the inflammation present in HD is primarily caused by activated microglia or an alternate source.

Pexidartinib (PLX3397) is a compound that is used to eliminate tumor-associated macrophages and microglia (Elmore, Lee et al. 2015). It is a tyrosine kinase receptor inhibitor, with strong affinities for colony stimulating factor 1 receptor (CSF1R), KIT proto-oncogene receptor tyrosine kinase (cKIT), and fms-like tyrosine kinase 3 (FLT3) (El-Gamal, Al-Ameen et al. 2018). As it can readily bypass the blood-brain barrier without active transport, PLX3397 can easily reach microglia and inhibit tyrosine kinase receptors important for microglia function and survival (Zhang and Fedoroff 1998, DeBoy, Rus et al. 2010, El-Gamal, Al-Ameen et al. 2018). The main target of PLX3397 is CSF1R, which is primarily expressed in myeloid lineage cells, including microglia and macrophages (Elmore, Lee et al. 2015, El-Gamal, Al-Ameen et al. 2018). CSF1R KO or $CSF1R^{null/null}$ mouse models have reduced levels of tissue macrophages, including microglia (Barres, Freeman et al. 2015). However, PLX3397 treatment has not been found to deplete healthy macrophages or other myeloid-lineage cells that express CSF1R (Mok, Koya et al. 2014, Li, Li et al. 2017). In addition to their presence on microglia, cKIT is found on astrocytes and hematopoietic progenitors, while FLT3 is present on hematopoietic cells and dendritic cells (Zhang and Fedoroff 1997, DeBoy, Rus et al. 2010, Perdiguero, Klapproth et al. 2015). cKIT is important for microglia survival and maintaining their resting state, and is upregulated in activated microglia after injury (Zhang and Fedoroff 1998, Zhang and Fedoroff 1999). FLT3 is involved with the pro-inflammatory response of activated microglia, as blockage of FLT3 signaling *in vitro* in activated mouse microglia dampened the pro-inflammatory response in a dose-dependent manner (DeBoy, Rus et al. 2010).

PLX3397 can be used *in vitro* or *in vivo* (Elmore, Najafi et al. 2014). The most common route of application *in vivo* is through the diet, at a dosage of 290ppm, however the compound can be tolerated at higher doses – up to 1160ppm chow in mice – with no side effects (Elmore,

Najafi et al. 2014, Elmore, Lee et al. 2015, Li, Li et al. 2017, Li, Li et al. 2017). After 21 days of PLX3397 chow at 290ppm, C57BL/6/129 mice showed a 99% reduction of microglia, with a majority of the depletion (70-90%) within the first 7 days (Elmore, Najafi et al. 2014, Elmore, Lee et al. 2015, Rice, Spangenberg et al. 2015). This reduction is through apoptosis of microglia, not deactivation (Elmore, Najafi et al. 2014). However, the remaining $Iba1^+$ cells repopulate the brain after 3 days of halting the treatment, so PLX3397 must be continually administered for sustained microglia ablation (Elmore, Najafi et al. 2014, Elmore, Lee et al. 2015, Huang, Xu et al. 2018). Studies in healthy mice have found no cognitive nor behavioural differences between adult mice taking PLX3397 or vehicle, nor are there any other notable side effects, even after 3 months of continual treatment (Elmore, Najafi et al. 2014, Rice, Spangenberg et al. 2015, Sosna, Philipp et al. 2018). Additionally, there are no cognitive, behavioural, nor motor changes after the mice are taken off PLX3397 and the microglia are allowed to re-populate (Elmore, Lee et al. 2015). PLX3397 is currently in phase 3 of clinical trials for cancer treatment (Daiichi Sankyo 2015).

PLX3397-induced microglia ablation has helped reduce disease-related symptoms in rodent models of other neurodegenerative diseases. Microglial ablation (~80%) using PLX3397 in the 5xfAD mouse model of Alzheimer's Disease led to improved contextual memory, reduced neuroinflammation, and prevented neuronal loss after 1 month of treatment, and decreased proteins that are hallmark to the disease after 3 months of treatment (Spangenberg, Lee et al. 2016, Sosna, Philipp et al. 2018). Furthermore, 90% microglia depletion after 21 days of PLX3397 treatment led to reduced inflammatory proteins (IL1α, IL1β, IL6, IFNγ, GM-CSF) in mice after intracerebral hemorrhage without altering their baseline expression prior to injury (Li, Li et al. 2017). PLX3397 treatment for 2 months in a spinocerebellar ataxia type 1 (SCA1) – another neurodegenerative disease caused by a polyglutamine gene mutation – mouse model, ATXN1[82Q], reduced microglia density by 82%, improved motor coordination, and decreased TNFα expression (Qu, Johnson et al. 2017). Furthermore, PLX3397 treatment in the 6-OHDA rat model of Parkinson's Disease decreased Iba1 protein levels by 72%, improved depressive-like behaviour and motor symptoms, and partially recovered their dopamine neurotransmission (Oh, Ahn et al. 2020).

While it is known that mhtt causes HD, the connection between mhtt and motor dysfunction, cognitive impairments, and neuropsychiatric symptoms is unknown (Roos 2010).

One aspect that mhtt alters is microglia functionality, including hyperactivity to stimulus (Kwan, Träger et al. 2012, Crotti, Benner et al. 2014, Savage, St-Pierre et al. 2020). However, although activated microglia are present in both HD patients and the R6/2 mouse model, current knowledge on the role of microglia in HD pathogenesis is limited to correlative data linking it to inflammation and neuronal death. Based off of literature from other neurodegenerative diseases, prolonged microglia activation appears to exacerbate neural degeneration in the region they are chronically active in (Lull and Block 2010). PLX3397-induced microglia ablation in the Alzheimer's Disease, SCA1, and Parkinson's Disease rodent models led to improvements in certain aspects of pathogenesis, such as reducing neuronal loss and improving motor function (Spangenberg, Lee et al. 2016, Qu, Johnson et al. 2017, Sosna, Philipp et al. 2018, Oh, Ahn et al. 2020). Therefore, to discern whether chronically active microglia play a similar detrimental role in HD progression, PLX3397-induced microglia ablation in the R6/2 mouse model was used to assess the extent of the degenerative or reparative effects of microglia on HD symptoms.

We hypothesized that continuous PLX3397 administration through chow at 290ppm *ad libitum* for 3 or more weeks would cause substantial microglia depletion in the R6/2 model, which would slow or halt HD progression in R6/2 mice. To assess our hypotheses, PLX3397 chow was provided to R6/2 mice for 5.5 weeks to deplete their microglia, and their disease progression was monitored using behavioural tests. The number of $Iba1^+$ microglia and their subtypes, $Nissl^+$ neurons, and parvalbumin interneurons in the neostriatum were quantified using immunohistochemistry and stereology to determine the extent of the PLX3397-induced microglia depletion, distribution of microglia subtypes, and striatal neuron survival.

2.3 Methods

2.3.1 Animals

R6/2 mice were bred from ovarian transplanted females (B6CBA-Tg(HDexon1)62Gpb/3J) and B6CBAF1/J males (Jackson Laboratory). Male R6/2 pups were weaned and genotyped for the mHTT gene at 3 weeks.

2.3.2 Experimental Cohorts

Low-dose (R6/2)

Male R6/2 carriers received AIN-76A diet containing PLX3397 (Chemgood, USA) at 290ppm (Envigo, USA) or standard AIN-76A chow at 6 weeks to eat *ad libitum* until the experimental endpoint at 11.5 weeks (PLX3397: n = 5, vehicle: n = 4). Behavioural experiments began at 6 weeks. Body and food weight were recorded every week.

Low-dose (WT)

Male B6CBAF1/J wildtypes (Jackson Laboratory) received AIN-76A diet containing PLX3397 at 290ppm or standard AIN-76A chow at 6 weeks to eat *ad libitum* until 9 weeks (PLX3397: n = 5, vehicle: n = 5). Body and food weight were recorded every week.

High-dose

Male R6/2 wildtype (WT) and carrier mice (CAR) received AIN-76A diet containing PLX3397 at 600ppm or standard AIN-76A chow at 6 weeks to eat *ad libitum* until 11.5 weeks (WT-vehicle: n = 10, WT-PLX3397: n = 7, CAR-vehicle: n = 7, CAR-PLX3397: n = 9). Behavioural experiments began at 4 weeks. Body and food weight were recorded every week. Brains were weighed post-perfusion.

2.3.3 Behavioural Tests

Clasping

Every week, the mice were assessed on their clasping score – a strong indicator of disease progression based on dystonia-like behaviour (Guyenet, Furrer et al. 2010, Samadi, Boutet et al. 2013). The mice were suspended by the base of their tail at a height of at least 30 cm and recorded twice for 20 seconds, with a 15 minute break in-between. Each individual limb was scored from 0 to 0.75 and tallied to form a total score from 0 to 3. The same criteria as Crevier-Sorbo *et al.* (2020) was applied: 0 for no clasping or climbing on the experimenter's hand; 0.25 for mild clasping – the limb retracts towards the midline of their body but does not reach and is unsustained; 0.5 for moderate clasping – the limb reaches the midline but is not sustained, or partial limb retraction that is sustained for 5 or more seconds; and 0.75 for severe clasping – the limb is fully retracted and sustained for 5 or more seconds.

Inverted Grid

At 4, 6, 8, and 10 weeks, the mice underwent Kondziela's inverted screen test to ascertain their limb muscle strength (Deacon 2013). For the inverted screen task, the mouse was situated on a wire mesh and rotated head-first to hang upside-down above an enclosed box within 2 seconds. The mouse was scored from 1 to 5 based on the length of time before falling: 1 for 1-10 seconds, 2 for 11-25 seconds, 3 for 26-60 seconds, 4 for 60-90 seconds, and 5 for 90-120 seconds (Deacon 2013).

Open Field

At 4, 6, 8, and 11 weeks, the mice performed the open field test. For the procedure, the mouse was placed in an empty square-shaped test chamber and left alone for 75 minutes. ViewPoint VideoTrack (ViewPoint, USA) recorded the mouse movements, which were analyzed using EthoVision XT (Noldus, Netherlands). The first 15 minutes was spent acclimating to the new environment. The latter 60 minutes of the recordings were used to calculate spontaneous locomotor activity and exploratory behaviour based on the total distance travelled and average velocity (Tatem, Quinn et al. 2014).

Elevated Plus Maze

At 4, 6, and 10 weeks, the elevated plus maze was performed to test for open space-induced anxiety (Walf and Frye 2007, Komada, Takao et al. 2008). The plus maze was set-up with two closed arms opposite each other (high walls) and two perpendicular open arms (no walls). A mouse was placed in the middle of the maze and allowed to freely wander for 10 minutes while ViewPoint VideoTrack (ViewPoint, USA) recorded its movements. The maze was enclosed inside a barrier to limit contextual information from outside the maze. Anxiety-like behaviour was calculated using EthoVision XT (Noldus, Netherlands) based off the duration of time spent in the open arms and closed arms, as their motivation to explore novel environments conflicts with their preference for dark enclosed spaces (Walf and Frye 2007, Komada, Takao et al. 2008).

2.3.4 Tissue Processing

At the experimental endpoint, the mice were deeply anesthetized and systemically perfused with 100 mL 0.9% saline, followed by fixation using 100 mL 4% paraformaldehyde (PFA). Their brains were extracted and placed in vials with 4% PFA for 24 hours at 4°C. The solution was replaced with 30% sucrose for 72 hours at 4°C for cryoprotection, before being cut with a freezing microtome at a thickness of 40 μm. The free-floating sections were sequentially placed into 6 vials containing phosphate-buffered saline (PBS) and stored at 4°C. For long-term storage, slices were kept in anti-freeze at -20°C.

2.3.5 Immunohistochemistry and Nissl Staining

Immunohistochemistry

Sections in anti-freeze were warmed to room temperature before being washed 3 times with PBS, each wash taking 5 minutes on a shaker at 70 rpm. Unless otherwise noted, each of the following steps were performed at room temperature on a shaker at 90-100 rpm. The PBS was replaced with 5 mL of blocking solution for 1 hour. Then the sections had 1 PBS wash, before 2.5 mL of primary antibody solution was added to each vial and left at 4°C overnight at 70 rpm. Iba1 antibody (1:1000, rabbit, Wako) was used to detect the presence of microglia, while parvalbumin antibody (1:5000, P3088, mouse, Sigma-Aldrich) was used to detect parvalbumin

interneurons. The next day, the sections were washed 3 times with PBS. Then 2.5 mL biotinylated secondary antibody solution was added and left for 1 hour. For the Iba1 primary antibody, anti-rabbit IgG (1:200, goat, MJS BioLynx) was used, while anti-mouse IgG (1:200, horse, MJS BioLynx) was used against the parvalbumin antibody. After 3 PBS washes, 1.5 mL ABC solution was added to the sections for 1 hour. Afterwards, there were 3 PBS washes, followed by 2 mL of DAB solution with 2% hydrogen peroxidase for 12-15 minutes. The slices were then washed 6 times with PBS. A negative control group underwent the same procedures but without primary antibody present. The free-floating slices were later mounted on microscope slides and left to dry for 3 days before coverslipping.

Coverslipping

The slides were left in 80% ethanol overnight at 37°C. The next day, the slides were put into two 100% ethanol baths for 1 minute each, dipped into 2 xylene baths, and then immediately coverslipped.

Nissl Staining

The sections immunolabelled for parvalbumin were counterstained with Nissl before coverslipping. The slides were left in 80% ethanol overnight at 37°C. The next day, they were placed in 70% ethanol for 5 minutes, dipped twice in distilled water, and placed in 0.2% cresyl violet with acetyl alcohol (pH ~4.25) for 6 minutes. The excess Nissl was removed with distilled water for 2 minutes, 70% ethanol for 2 minutes, 95% ethanol with 0.07% acetyl alcohol for 2 minutes, followed by two 100% ethanol baths for 2 minutes each. The slides then were dipped into xylene before directly being coverslipped.

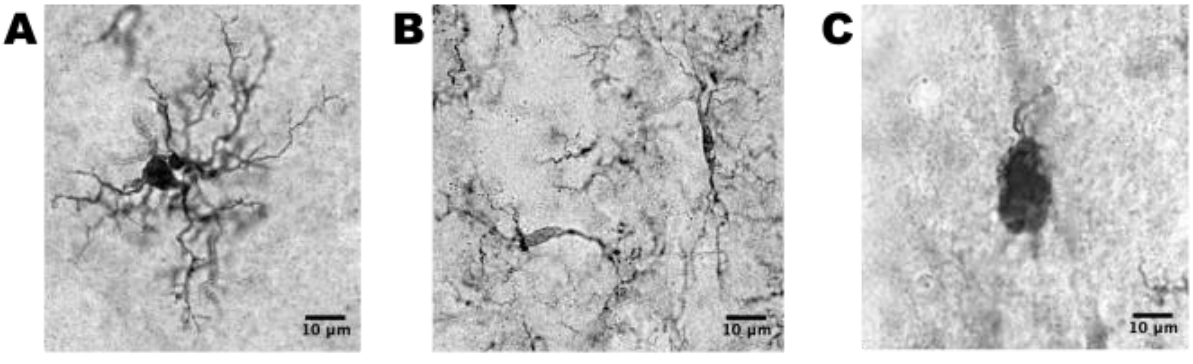

Figure 1. Microglia subtypes: **(a)** ramified, **(b)** intermediate, and **(c)** activated/amoeboid.

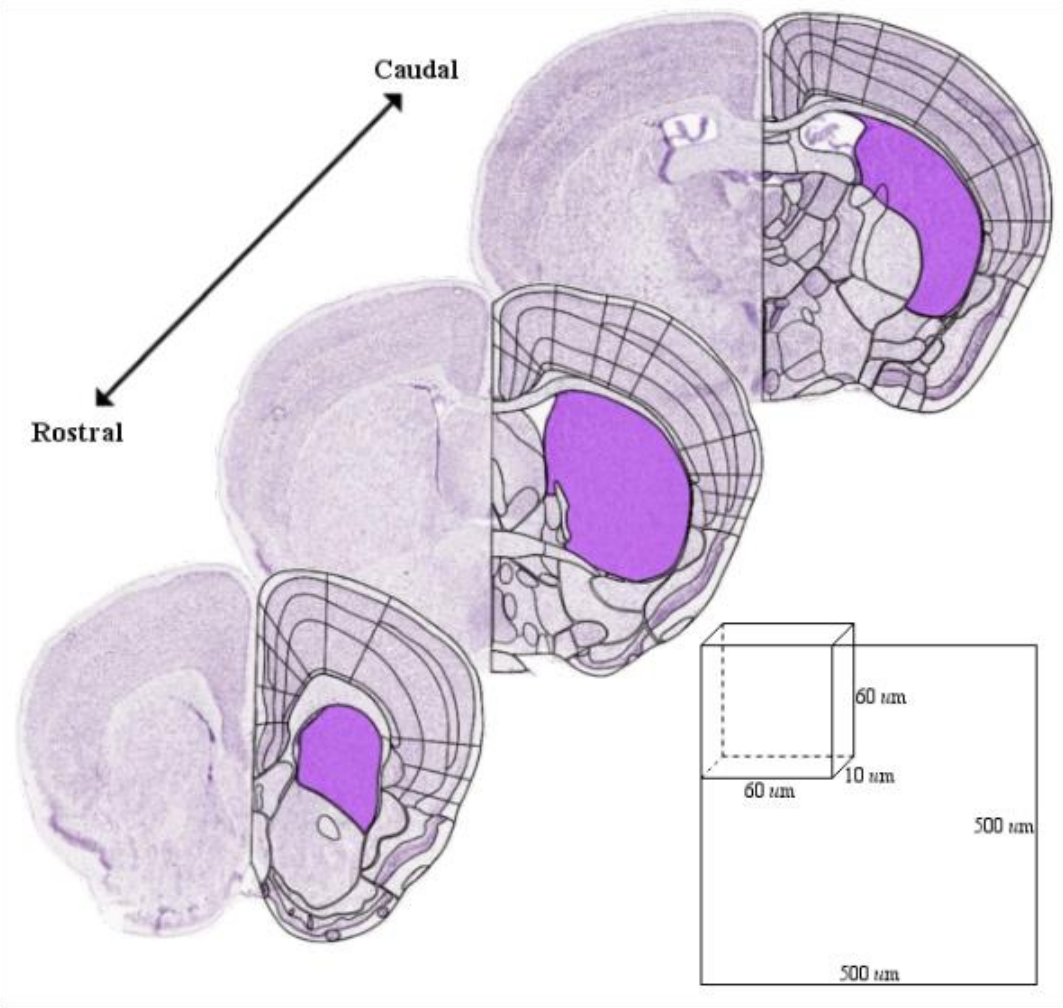

Figure 2. Schematic for stereological counting of Nissl+ neurons in the neostriatum. Images of mouse coronal sections obtained from the Allen Mouse Brain Atlas at mouse.brain-map.org/static/atlas (Image credit: Allen Institute). Stereological counting was performed on every sixth serial coronal section (240 µm intervals). For each coronal section, the neostriatum (unilateral) was divided into multiple 500 x 500 µm grids, and Nissl-positive neurons were counted within a 60 x 60 µm frame with a 10 µm dissector height per every grid (diagram not to scale).

2.3.6 Stereology

StereoInvestigator (MBF Bioscience, USA) was used to count microglia, parvalbumin (PV) interneurons, and Nissl-positive neurons in the neostriatum (unilateral) and ascertain the average cell body area of the microglia subtypes, via the optical fractionator and nucleator programs. It also provided neostriatum volume estimates. A light microscope with an attached camera was used. The neostriatum boundaries were defined based on boundaries outlined by Sadikot and Sasseville (1997) and The Mouse Brain in Stereotaxic Coordinates (Paxinos and Franklin 2004). Every sixth serial coronal section containing neostriatum was examined (240 μm intervals). The

microglia were counted under oil immersion with a 60X objective, with an optical fractionator brick size of 125 x 125 μm per 450 x 450 μm grid. Nissl-positive and PV neurons were counted with a 100X objective, with a frame size of 60 x 60 μm within a 500 x 500 μm grid (for Nissl) or 300 x 300 μm grid (for PV). The mean section thickness was set at 12 μm, providing 1 μm guard zones on the top and bottom of a 10 μm dissector height. The tissue thickness was measured every 5^{th} site, and nucleator every 5^{th} cell. The 4 microglia subtypes were divided into 3 groups based on the criteria outlined by Torres-Platas *et al.* (2014): ramified – cells with a small soma with many thin processes radiating in all directions with high order branching; intermediate – cells with a more elliptical cell body and fewer thin processes with less high order branching and/or thicker processes; and activated/amoeboid – cells with amoeboid cell bodies with little or no processes which have little or no branching. $Nissl^+$ cells were required to have at least a 7 μm diameter soma and a lighter cytoplasm with darker Nissl bodies to be counted as a neuron (Samadi, Boutet et al. 2013).

2.3.7 Statistical Analyses

Statistics were calculated using SPSS. Data is presented as mean ± standard error of the mean. Statistical significance was accepted at a p-value < 0.05 and is expressed as: $*p < 0.05$, $**p < 0.01$, $***p < 0.001$. Independent t-test was used to compare neostriatum volumes, total microglia, $Nissl^+$ striatal neurons, and PV interneurons for the Low-dose experiments. For the High-dose analysis, two-way ANOVA was used for comparisons of brain weight, neostriatum volume, total microglia, and microglia density. Body weight, microglia subtypes, and behavioural tests were analyzed using the two-way mixed ANOVA for the Low-dose experiments and the three-way mixed ANOVA for the High-dose experiment. Unless otherwise stated, the data showed no outliers based on assessment of studentized residuals (or boxplots for the t-tests), normal distribution based on Normal Q-Q Plots (or Shapiro-Wilk's test ($p > 0.05$) for the t-tests), and homogeneity of variances based on Levene's test ($p > 0.05$). Additionally, the two-way mixed ANOVAs showed homogeneity of covariances based on Box's test of equality of covariance matrices ($p > 0.001$). If Mauchly's test for sphericity of variance was violated in the mixed ANOVA, the Greenhouse-Geisser correction was used. For data sets containing non-normal distributions and/or heterogeneity of variances, a non-parametric equivalent to the

ANOVA was performed using ARTool in R which looked at the rank transformed data (Wobbrock, Findlater et al. 2011, Crevier-Sorbo, Rymar et al. 2020). The p-value for multiple comparisons were adjusted using Bonferroni corrections in SPSS or the Holm method in R.

2.4 Results

2.4.1 Mild microglia reduction did not alter neuropathology in the Low-dose (R6/2) experiment

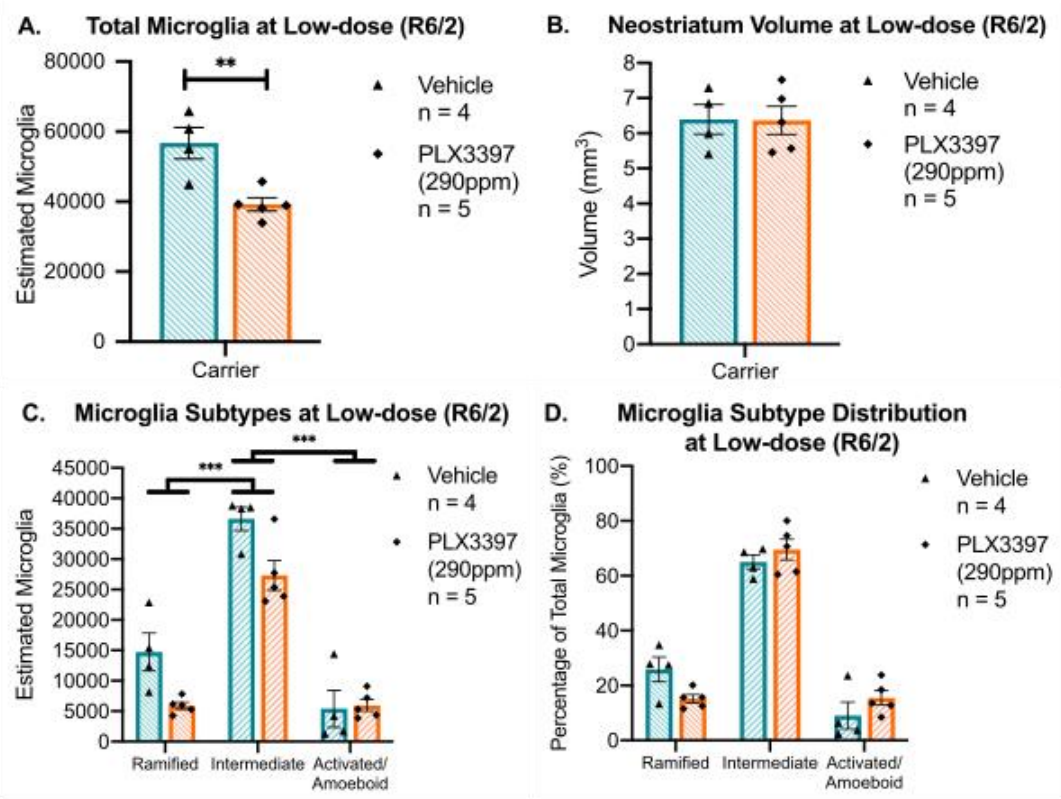

Figure 3. Mild microglia depletion occurred after R6/2 carriers received PLX3397 treatment at 290ppm for 5.5 weeks. **(a)** There was a significant 31% reduction in total microglia in the neostriatum at 11.5 weeks ($p = 0.006$), **(b)** which was not due to a change in the neostriatum volume ($p = 0.966$). **(c)** There was a trend for a different subtype distribution between treatment groups ($p = 0.079$), **(d)** which based on the relative amount of microglia subtypes, suggests a shift towards more activated phenotypes after PLX3397 treatment.

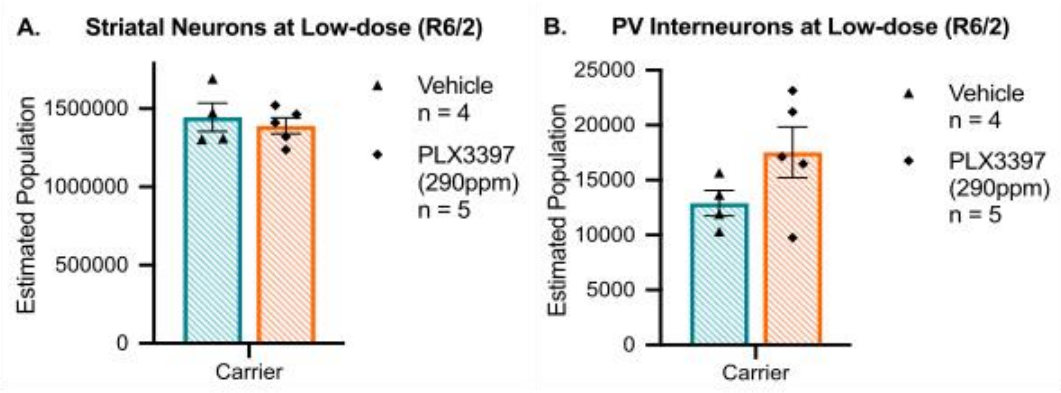

Figure 4. Striatal neuron survival did not significantly improve in R6/2 carriers in the Low-dose (R6/2) group. **(a)** Nissl-positive striatal neuron numbers were no different between treatment groups at 11.5 weeks ($p = 0.597$), **(b)** however, a non-significant 36% increase in parvalbumin (PV) interneuron numbers in the neostriatum was detected in the PLX3397 group ($p = 0.143$).

Treatment of PLX3397 at 290ppm for 5.5 weeks resulted in a 31% reduction of microglia in the neostriatum of R6/2 carriers compared to the control group (Fig. 3a; Table 2; $t(7) = 3.904$, $p = 0.006$, $d = 2.62$), which was lower than the level of depletion expected based on the literature. There were two outliers in the PLX3397 group for total microglia which were kept in the analysis due to the limited number of samples. The difference in total microglia was not due to a difference in neostriatum volume between treatment groups (Fig. 3b; $t(7) = 0.044$, $p = 0.966$, $d = 0.03$).

The depletion primarily affected ramified microglia (-60%) and intermediate microglia (-25%), whereas there was a slight increase in the activated/amoeboid subtype (+10%) (Fig. 3c; Table 2). While this suggests a shift towards more activated phenotypes after receiving PLX3397 (Fig. 3d), the effects of treatment on subtype distribution was non-significant ($F(2,14) = 3.05$, $p = 0.079$, partial $\eta^2 = 0.304$). There were significant differences between the estimated microglia subtype populations ($F(2,14) = 78.06$, $p < 0.001$, partial $\eta^2 = 0.918$), with the vast majority of R6/2 microglia belonging to the intermediate group compared to the ramified ($p < 0.001$) or activated/amoeboid categories ($p < 0.001$). As expected, the total number of microglia between treatment groups was also significantly different ($F(1,7) = 15.24$, $p = 0.006$, partial $\eta^2 = 0.685$).

Although there was a reduction in microglia, there was no reciprocal change in striatal neuron numbers due to PLX3397 treatment at 290ppm (Fig. 4a; Table 3; $t(7) = 0.554$, $p = 0.597$, $d = 0.37$). Conversely, there was a trend for increased PV interneuron survival after microglia depletion as indicated by the non-significant 36% increase in PV interneurons in the treated group (Fig. 4b; Table 3; $t(7) = -1.652$, $p = 0.143$, $d = 1.11$).

Table 2. Number of microglia in the neostriatum of 11.5-week-old R6/2 carriers from the Low-dose (R6/2) experiment and 9-week-old wildtype mice from the Low-dose (WT) experiment.

	R6/2 Carrier (11.5 weeks)			**Wildtype (9 weeks)**		
	Vehicle	**PLX3397 (290ppm)**	**Microglia Depletion**	**Vehicle**	**PLX3397 (290ppm)**	**Microglia Depletion**
Total	56717 ± 4495	39182 ± 1888	31%*	71555 ± 5591	46134 ± 2099	36%**
Ramified	14706 ± 3107	5903 ± 584	60%	-	-	-
Intermediate	36610 ± 1924	27322 ± 2447	25%	-	-	-
Activated/ Amoeboid	5400 ± 3070	5957 ± 966	-10%	-	-	-

*p < 0.05, **p < 0.01, ***p < 0.001

Table 3. Number of neurons in the neostriatum of 11.5-week-old R6/2 carriers from the Low-dose (R6/2) experiment.

	R6/2 Carrier (11.5 weeks)		
	Vehicle	**PLX3397 (290ppm)**	**Neuron Survival**
Total Striatal Neurons	1445058 ± 91082	1390636 ± 50280	-4%
Parvalbumin Interneurons	12896 ± 1149	17530 ± 2309	36%

*p < 0.05, **p < 0.01, ***p < 0.001

2.4.2 Behavioural symptoms were not rescued by microglia depletion in the Low-dose (R6/2) experiment

Although there was a 31% reduction in microglia by 11.5 weeks, the PLX3397 group showed no improvement in their behavioural symptoms compared to the control group. Both treatment groups showed the same progressive pattern of clasping behaviour (Fig. 5a; $F(5) = 0.30$, $p = 0.913$), which significantly worsened over time for both groups ($F(5) = 9.53$, $p < 0.001$). Treatment had no effect over time on limb muscle strength (Fig. 5b; $F(2) = 0.24$, $p = 0.787$), which gradually weakened in both cohorts ($F(2) = 25.64$, $p < 0.001$). Furthermore, both treatment groups showed a progressive decline in total distance travelled in the open field (Fig. 5c; $F(2, 12) = 19.32$, $p < 0.001$, partial $\eta^2 = 0.763$), particularly between weeks 6 and 8 ($p < 0.001$) and weeks 6 and 11 ($p = 0.009$), which was not improved by PLX3397 treatment over time ($F(2, 12) = 0.41$, $p = 0.672$, partial $\eta^2 = 0.064$). Note that a mouse in the vehicle group had to be excluded from the open field analysis due to equipment malfunction. The treatment groups also did not differ in anxiety-like behaviour over time based on the duration spent in the closed arms (Fig. 5d; $F(1, 7) = 0.08$, $p = 0.783$, partial $\eta^2 = 0.012$) or open arms of the elevated plus maze (Fig. 5e; $F(1, 7) = 0.68$, $p = 0.436$, partial $\eta^2 = 0.089$), nor were there general changes in behaviour with age (closed: $F(1, 7) = 0.06$, $p = 0.783$, partial $\eta^2 = 0.009$; open: $F(1, 7) = 1.80$, $p = 0.222$, partial $\eta^2 = 0.204$).

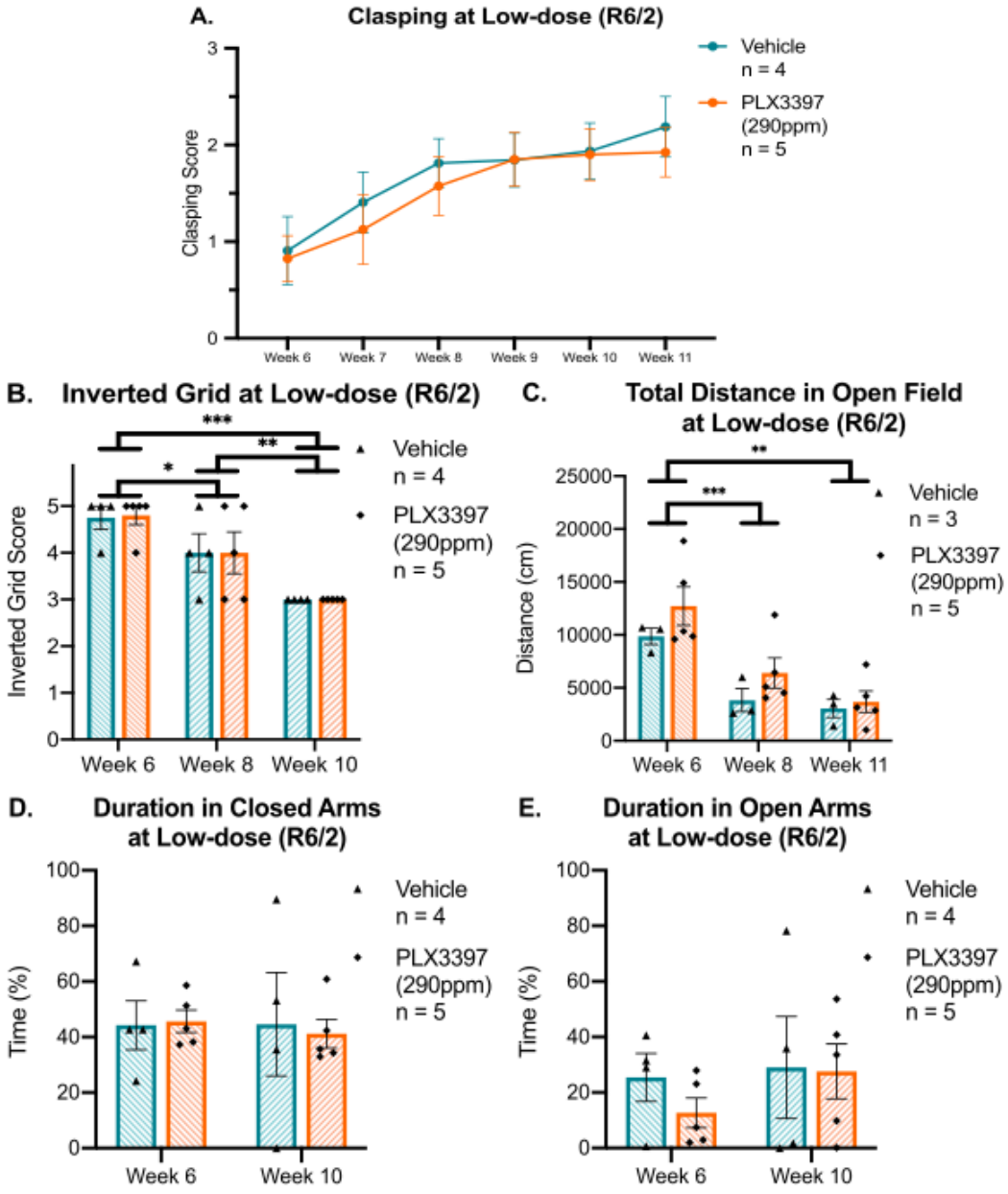

Figure 5. Behavioural progression of Huntington's Disease in R6/2 carriers did not change due to PLX3397 treatment at 290ppm in the Low-dose (R6/2) experiment. The treated group showed no improvements over time on **(a)** clasping score ($p = 0.913$), **(b)** inverted grid score ($p = 0.787$), **(c)** distance travelled in the open field ($p = 0.672$), nor **(d, e)** time spent in the closed and open arms of the elevated plus maze (closed: $p = 0.783$; open: $p = 0.436$).

2.4.3 Extent of microglia depletion lower than expected in the Low-dose (WT) group

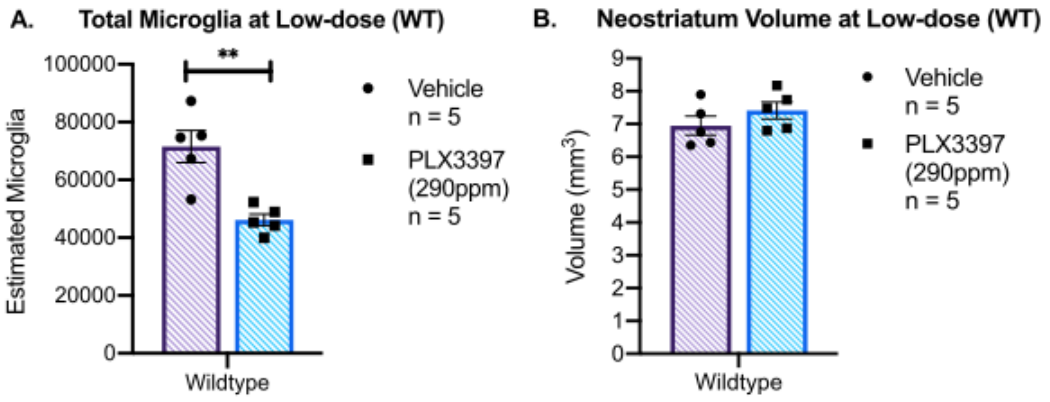

Figure 6. The extent of microglia depletion in wildtype mice after 3 weeks of PLX3397 at 290ppm in the Low-dose (WT) group were closer to the levels seen in the Low-dose (R6/2) experiment than in the literature. **(a)** Total microglia numbers were reduced by 36% in the neostriatum of 9 week old wildtype mice ($p = 0.003$), **(b)** which was not due to a difference in their neostriatum volumes ($p = 0.749$).

Even after the 3-week minimum for maximal microglia depletion using PLX3397 at 290ppm, there was only a 36% reduction in total microglia in the neostriatum of wildtype mice (Fig. 6a; Table 2; $t(8) = 4.257$, $p = 0.003$, $d = 2.69$). This was much lower than the levels seen in other wildtype mice in the literature (Table 1). There was one outlier in the vehicle group for total microglia which was kept in the analysis due to the limited number of samples. The reduction in microglia was not due to a change in neostriatum volume between treatment groups (Fig. 6b; $t(8) = -1.183$, $p = 0.749$, $d = 0.75$).

2.4.4 PLX3397-induced microglia depletion was less effective in R6/2 carriers than wildtype littermates in the High-dose experiment

To heighten the microglia depletion, the PLX3397 chow concentration was increased from 290ppm to 600ppm for the High-dose experiment. However, the response to PLX3397 treatment at 600ppm was significantly different between the genotypes (Fig 7a; $F(1) = 27.49$, $p < 0.001$), with the total microglia being reduced by only 57% in R6/2 carriers ($p < 0.001$) but 91% in wildtype littermates ($p < 0.001$). Furthermore, there was not only a significant genotypic difference in total microglia between the treated groups ($p = 0.002$), but also the vehicle groups ($p = 0.010$). Neostriatum volume differed according to both genotype and treatment groups (Fig

7b; $F(1, 29) = 7.24$, $p = 0.012$, partial $\eta^2 = 0.200$). As the estimated neostriatum volume was 15% smaller in R6/2 carriers than wildtype controls ($p = 0.002$), microglia density was also analyzed (Supplementary Fig. S4). The microglia density further solidified that the treatment response was different between the genotypes ($F(1) = 22.48$, $p < 0.001$). Whereas the density was the same between the genotypes in the vehicle groups ($p = 0.962$), the treated wildtype group had a lower microglia density compared to the treated carrier group ($p < 0.001$). While there was a difference in estimated neostriatum volume between the wildtype cohorts (Fig. 7b; $p = 0.028$), brain weight only differed based on genotype (Fig. 7e; $F(1, 29) = 26.54$, $p < 0.001$, partial $\eta^2 = 0.478$).

The effectiveness of PLX3397-induced depletion on each microglia subtype varied depending on the genotype (Fig 7c; Table 4; $F(2) = 20.91$, $p < 0.001$). Subtype distribution was significantly different between treatment groups for both R6/2 carriers ($F(2) = 37.30$, $p < 0.001$) and wildtype littermates ($F(2) = 170.29$, $p < 0.001$). Similar to the Low-dose (R6/2) experiment, R6/2 carriers in the High-dose experiment showed a substantial depletion of their ramified (70%; $p < 0.001$) and intermediate subtypes (56%; $p < 0.001$), while the activated/amoeboid microglia non-significantly increased by 46% ($p = 0.174$). On the other hand, wildtype mice showed substantial depletion in all subtypes (78-92%; $p < 0.001$), with the least being for the activated/amoeboid subtype (78%). This may suggest that more activated microglia are less susceptible to PLX3397, or the process of PLX3397-induced depletion shifts microglia towards activation (Fig. 7d). Subtype distribution also differed based on genotype ($F(2) = 104.87$, $p < 0.001$). Between the vehicle groups, R6/2 carriers had 39% less ramified microglia ($p < 0.001$) and 30% more intermediate microglia ($p < 0.001$), with no significant change in activated/amoeboid microglia ($p = 0.740$). The altered distribution of microglia subtypes between vehicle groups indicates increased microglia activation in the R6/2 model at baseline.

Table 4. Number of microglia in the neostriatum of 11.5-week-old R6/2 carriers and wildtype littermates from the High-dose experiment.

	R6/2 Wildtype (11.5 weeks)			**R6/2 Carrier (11.5 weeks)**		
	Vehicle	**PLX3397 (600ppm)**	**Microglia Depletion**	**Vehicle**	**PLX3397 (600ppm)**	**Microglia Depletion**
Total	69356 ± 1646	6325 ± 2753	91%***	59230 ± 2716	25401 ± 3430	57%***
Ramified	43722 ± 1121	3513 ± 1567	92%***	26689 ± 2002	7996 ± 1106	70%***
Intermediate	22721 ± 1132	2181 ± 1128	90%***	29563 ± 1266	13063 ± 2202	56%***
Activated/ Amoeboid	2913 ± 267	631 ± 92	78%***	2978 ± 644	4342 ± 896	-46%

*p < 0.05, **p < 0.01, ***p < 0.001

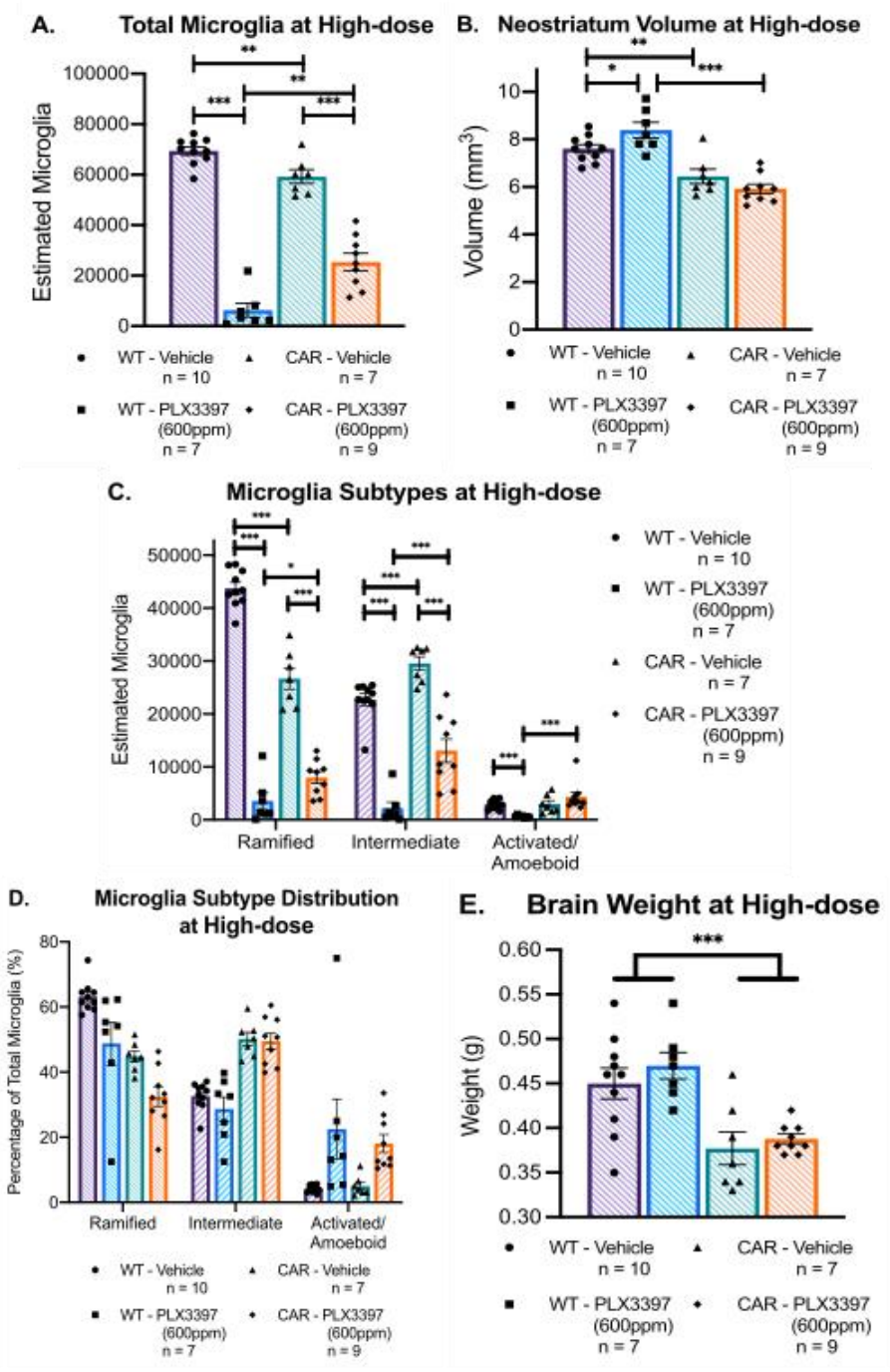

Figure 7. Greater microglia depletion was seen in wildtype littermates compared to R6/2 carriers after 5.5 weeks of PLX3397 chow at 600ppm. **(a)** Microglia numbers in the neostriatum were reduced by 91% in wildtypes ($p < 0.001$) and 57% in carriers ($p < 0.001$) after treatment. R6/2 carrier controls had 15% less microglia compared to wildtype littermates ($p = 0.010$), **(b)** but also had on average a 15% smaller neostriatum volume ($p = 0.002$). **(c)** Subtype distribution was significantly different between the genotypes in the vehicle groups ($p < 0.001$) and changed after treatment for both wildtypes ($p < 0.001$) and carriers ($p < 0.001$). **(d)** The relative subtype distribution visualizes the increased microglia activation in R6/2 carriers compared to vehicle wildtype littermates, which was increased after PLX3397 treatment for both genotypes. **(e)** Brain weight was 16% lighter in carriers compared to wildtype mice ($p < 0.001$).

2.4.5 Higher levels of microglia depletion did not improve behavioural symptoms in the High-dose group

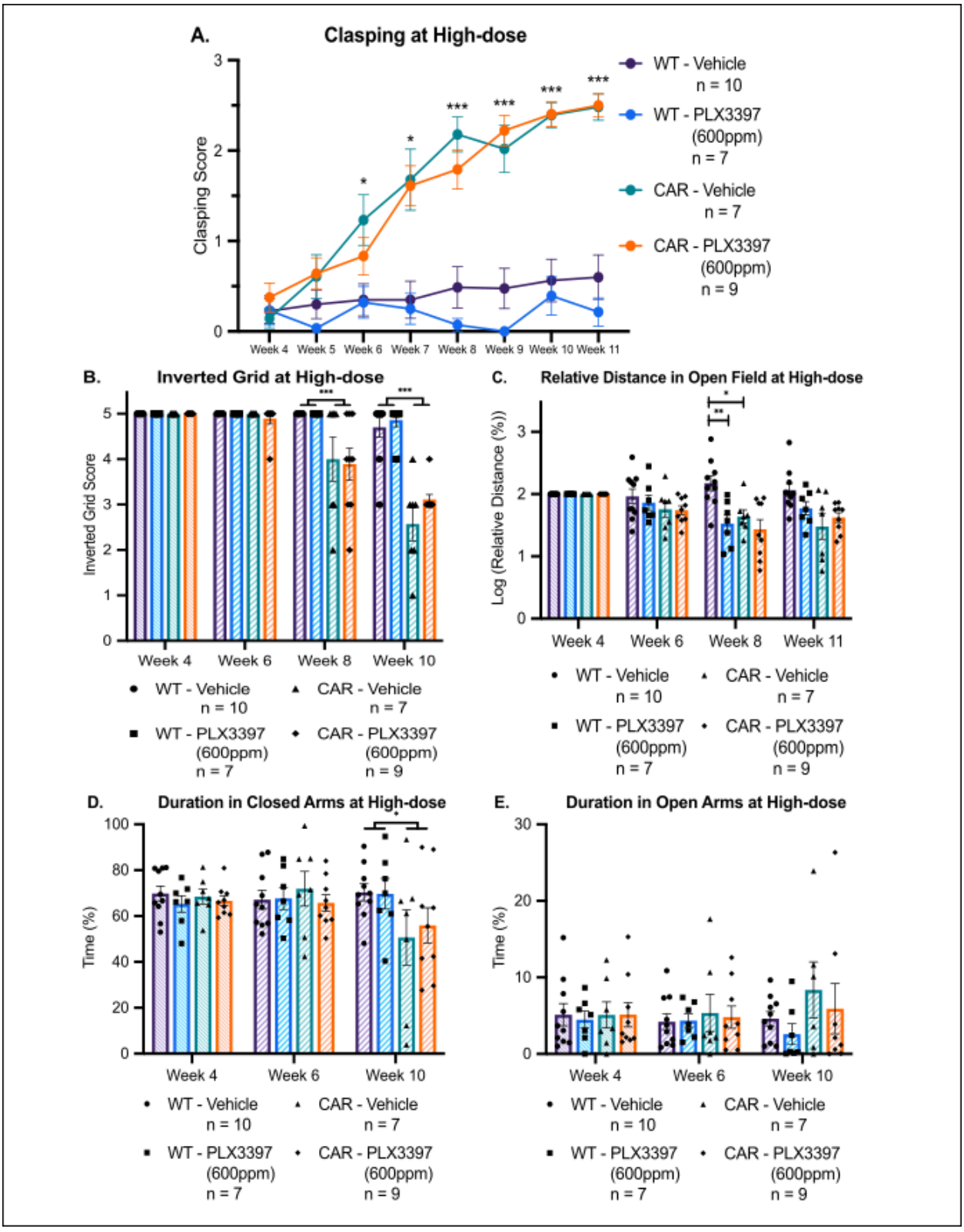

Figure 8. R6/2 carriers followed the expected pattern of behavioural symptoms for Huntington's Disease compared to wildtype littermates, which did not improve due to PLX3397 treatment at 600ppm for 5.5 weeks. **(a)** There was a three-way interaction between treatment, genotype, and time on clasping scores ($p = 0.016$), however treatment did not change either the carrier's nor the wildtype's scores over time (WT $p = 0.284$; CAR $p = 0.341$). Vehicle R6/2 carriers preformed poorer than wildtype littermates with age ($p < 0.001$), especially after 6 weeks (4w $p = 0.910$, 5w $p = 0.369$, 6w $p = 0.019$, 7w $p = 0.010$, 8w-11w $p < 0.001$). **(b)** The three-way interaction was non-significant for inverted grid scores ($p = 0.224$). R6/2 carriers overall preformed progressively worse than their wildtype counterparts ($p < 0.001$; 6w $p = 0.332$, 8w and 10w $p < 0.001$). There were significant differences in the pattern of decline between treatment groups ($p < 0.001$), but none of the timepoints were significantly different (6w and 8w $p = 0.935$, 10w $p = 0.954$). **(c)** The relative distance travelled in the open field had a significant three-way interaction ($p < 0.001$), however further analysis found that only the treated wildtype group preformed worse over time (WT $p = 0.005$; CAR $p = 0.815$), particularly at 8 weeks (6w $p = 0.475$, 8w $p = 0.009$, 11w $p = 0.176$). Between vehicle groups, R6/2 carriers showed less spontaneous movement over time compared to wildtype littermates ($p = 0.009$), especially at 8 weeks (6w $p = 0.417$, 8w $p = 0.029$, 11w $p = 0.140$). **(d, e)** There were no significant three-way interactions for the duration spent in the closed nor open arms of the elevated plus maze (closed $p = 0.546$; open $p = 0.840$). R6/2 carriers overall showed progressively less anxiety-like behaviour with age based on their time in both the closed ($p = 0.026$; 4w $p = 1.000$, 6w $p = 0.786$, 10w $p = 0.036$) and open arms ($p = 0.043$; 4w, 6w and 10w $p = 1.000$). There were no changes between treatment groups over time (closed $p = 0.576$; open $p = 0.671$).

The behavioural pattern of untreated R6/2 carriers and wildtype littermates matched the literature. Dystonia-like behaviour significantly worsened for vehicle R6/2 carriers over time (Fig. 8a; $F(7) = 25.61$, $p < 0.001$), with pronounced divergence from the vehicle wildtype scores beginning at 6 weeks (4w $p = 0.910$, 5w $p = 0.369$, 6w $p = 0.019$, 7w $p = 0.010$, 8w-11w $p < 0.001$). Limb muscle strength also declined in carriers (Fig. 8b; $F(3) = 48.75$, $p < 0.001$), notably at weeks 8 and 10 (6w $p = 0.332$, 8w and 10w $p < 0.001$). As the raw values for the total distance travelled in the open field showed high variability, the raw data was transformed to use week 4 (i.e. pre-treatment) as each mouse's individual baseline before making group comparisons. The relative distance travelled decreased over time for vehicle carriers compared to vehicle wildtype mice (Fig. 8c; $F(3) = 4.31$, $p = 0.009$), which was most pronounced at 8 weeks (6w $p = 0.417$, 8w $p = 0.029$, 11w $p = 0.140$). The R6/2 carriers showed less anxiety-like behaviour over time based on their duration spent in the closed arms (Fig. 8d; Greenhouse-Geisser correction: $F(1.378, 39.976) = 4.65$, $p = 0.026$, partial $\eta^2 = 0.138$), specifically at week 10 (4w $p = 1.000$, 6w $p = 0.786$, 10w $p = 0.036$), and open arms of the elevated plus maze (Fig. 8e; $F(2) = 3.34$, $p = 0.043$; 4w, 6w and 10w $p = 1.000$).

Increased levels of microglia depletion due to a higher dose of PLX3397 (600ppm) still did not improve the behavioural symptoms in R6/2 carriers. Even though the clasping score analysis revealed that the genotypes had a different response to PLX3397 treatment over time (Fig. 8a; $F(7) = 2.49$, $p = 0.016$), further analysis showed that dystonia-like behaviour did not progressively improve or change from treatment in carrier mice ($F(7) = 1.14$, $p = 0.341$) nor wildtype mice ($F(7) = 1.24$, $p = 0.284$). For both genotypes, both treatment groups displayed worsening scores over time, however the effect was much larger in carrier mice (CAR: $F(7) = 58.45$, $p < 0.001$; WT: $F(7) = 2.22$, $p = 0.034$). Inverted grid scores showed no three-way

interaction between genotype, treatment, and time (Fig. 8b; $F(3) = 1.49$, $p = 0.224$). Overall, there were significant differences in limb muscle strength over time between treatment groups ($F(3) = 12.22$, $p < 0.001$), but there were no specific timepoints with significant differences (6w and 8w $p = 0.935$, 10w $p = 0.954$). Wildtype and carrier mice behaved differently in the open field in response to continuous PLX3397 treatment (Fig. 8c; $F(3) = 6.04$, $p < 0.001$). Spontaneous locomotor activity in the open field did not improve over time for treated carrier mice ($F(3) = 0.31$, $p = 0.815$), which progressively decreased alongside the carrier controls ($F(3) = 16.29$, $p < 0.001$). The open field test also revealed a possible side effect of PLX3397, as the treated wildtype group performed worse than their control cohort over time ($F(3) = 4.85$, $p = 0.005$), particularly at 8 weeks (6w $p = 0.475$, 8w $p = 0.009$, 11w $p = 0.176$). There were no genotype and treatment interactions over time for the duration spent in the closed arms (Fig. 8d; Greenhouse-Geisser correction: $F(1.378, 39.976) = 0.49$, $p = 0.546$, partial $\eta^2 = 0.017$) nor open arms of the elevated plus maze (Fig. 8e; $F(2) = 0.17$, $p = 0.840$). Treatment did not progressively alter anxiety-like behaviour based on the time spent in the closed (Greenhouse-Geisser correction: $F(1.378, 39.976) = 0.44$, $p = 0.576$, partial $\eta^2 = 0.015$) and open arms ($F(2) = 0.40$, $p = 0.671$).

2.5 Discussion

To assess the role microglia play in HD progression, microglia were pharmaceutically ablated in the R6/2 model of HD and their behaviour was monitored using the clasping test, inverted grid, open field, and elevated plus maze. Furthermore, striatal neuropathology was stereologically assessed as the neostriatum is the region most affected by neuronal atrophy in HD, with striatal neuron loss correlating with movement impairment severity (Roze, Cahill et al. 2011, Guo, Rudow et al. 2012). The administration of PLX3397 via chow *ad libitum* – set at the same dose which resulted in 99% microglia ablation in wildtype mice (i.e. 290ppm) – was expected to lead to similar levels of microglia depletion in R6/2 mice after a minimum of 21 days (Table 1; Elmore, Najafi et al. 2014). However, in the Low-dose (R6/2) experiment, there was only a 31% decrease in total $Iba1^+$ microglia in the neostriatum of R6/2 carriers after 5.5 weeks of PLX3397 treatment at 290ppm ($p = 0.006$). Treatment did not negatively affect their body weight or neostriatum volume, however, there were also no motor or behavioural improvements, nor increased neuronal survival (Supplementary Fig. S2).

To assess if the lower-than-expected microglia depletion was due to a lower drug response in mhtt carriers, wildtype (B6CBAF1/J) mice with a similar genetic background to the R6/2 model were given PLX3397 chow at the same dose of 290ppm for 3 weeks to try replicating the 99% depletion seen by Elmore *et al.* (2014). However, similar to the Low-dose (R6/2) experiment, the wildtype mice only had a 36% decrease in total $Iba1^+$ microglia ($p = 0.003$), and again, treatment did not affect body weight nor neostriatum volume (Supplementary Fig. S2). This is unlikely to be an issue with the PLX3397 compound as it was sourced from the same company used by Oh *et al.* (2020), who showed a large 72% Iba1 reduction in the 6-OHDA Parkinson's Disease rodent model. Therefore, providing PLX3397 in chow *ad libitum* does not reliably provide the continuous dosage required for maximal depletion in R6/2 mice. Bennett *et al.* (2018) also found that PLX3397 treatment at 290ppm for 3 months resulted in a 30% reduction in $Iba1^+$ microglia in the Tg4510 mouse model for Alzheimer's Disease and their wildtype littermates, and similarly, saw no improvements in cellular pathology (Table 1)**.** One wildtype mouse with a 96% reduction had a heavier body weight than its littermates, further suggesting the difference in microglia reduction had to do with inconsistent dosing (Bennett, Bryant et al. 2018).

As 31% microglia depletion was not sufficient to significantly alter the neurodegenerative or behavioural aspects of HD, R6/2 mice – both carriers and wildtype littermates – were subjected to PLX3397 at a higher dose of 600ppm. The compound was still provided in chow *ad libitum* to maintain consistency with the initial study. Whereas R6/2 wildtype mice reached close to the desired level of complete depletion with a 91% decrease in total microglia ($p < 0.001$), R6/2 carriers were less responsive to PLX3397 as microglia only decreased by 57% ($p < 0.001$). Again, treatment at a higher dose did not have a large effect on body weight, neostriatum volume, nor post-perfused brain weight (Supplementary Fig. S2). However, there were still no improvements in the behavioural symptoms of R6/2 carriers even after increasing the amount of microglia depletion.

2.5.1 Untreated R6/2 mice followed their predicted biometric and behavioural patterns

Body weight, neostriatum volume, and brain weight matched the R6/2 literature. Wildtype mice continued to gain substantially more body weight over time compared to carriers between the vehicle groups (Supplementary Fig. S2; $p < 0.001$). Although there were no significant differences at specific timepoints like Samadi *et al.* (2013) saw from 9 weeks onwards, we did see a plateauing of body weight in R6/2 carriers around 7 weeks like Crapser *et al.* (2020). R6/2 carriers had on average a 15% smaller neostriatum volume ($p = 0.002$) and a 16% lighter brain weight ($p < 0.001$) compared to wildtype littermates at 11.5 weeks, which was likely due to HD-related neurodegeneration. The neostriatum volume and brain weight values matched those of age-matched R6/2 mice in the literature (Davies, Turmaine et al. 1997, Samadi, Boutet et al. 2013).

The general motor decline in R6/2 carriers compared to their wildtype littermates mirrored Samadi *et al.* (2013). Clasping scores started to deviate between genotypes at 6 weeks rather than the expected 4 weeks due to our wildtype littermates having higher baseline scores (Samadi, Boutet et al. 2013). Muscle strength and spontaneous locomotor activity started decreasing at 8 weeks, which was similar to the expected 9 weeks for muscle strength and 7 weeks for the distance travelled in the open field (Samadi, Boutet et al. 2013). R6/2 carriers showed signs of a progressive reduction in anxiety-like behaviour. This was indicated by their progressively diminishing time in the closed arms of the elevated plus maze ($p = 0.026$),

especially at 10 weeks ($p = 0.036$), coinciding with an increasing duration spent in the open arms ($p = 0.043$). Their reduced anxiety-like behaviour was expected as R6/2 carriers have shown increased duration in the open arms starting from 8 weeks compared to their wildtype littermates (File, Mahal et al. 1998).

2.5.2 Microglia depletion does not have pronounced therapeutic potential in the R6/2 model

Both treatment groups from the Low-dose (R6/2) experiment followed the same pattern of motor decline for clasping, inverted grid, and open field, and there were no changes in their anxiety-like behaviour based on the elevated plus maze. The estimated $Nissl^+$ striatal neuron population for the untreated cohort matched the predicted amount for R6/2 carriers in the literature, and there was no change in their numbers due to treatment (Samadi, Boutet et al. 2013). There was a trend for increased parvalbumin interneuron survival in R6/2 carriers receiving treatment, but the lack of significance may be due to the experiment not being powered adequately. To help address that issue, the cohort sizes were increased for the High-dose experiment in addition to the increased PLX3397 dose. However, even with higher levels of microglia depletion in the High-dose experiment, R6/2 carriers still showed no motor improvements in terms of dystonia-like behaviour, muscle strength, and spontaneous locomotor activity, nor changes in their anxiety-like behaviour. Considering that an increase in microglia ablation did not have a reciprocal effect on behaviour, this indicates that microglia do not play a pronounced role in HD symptoms.

While PLX3397 treatment resulted in no change in the behaviour of wildtype mice for most tests, the treated group performed poorer than controls in the total distance travelled in the open field ($p = 0.005$). This side effect of PLX3397 may have elucidated Elmore *et al.* (2014) as our open field test ran for a longer duration, thus possibly capturing finer changes in their behaviour.

Another recent study by Crapser *et al.* (2020) also looked at the effects of microglia depletion in R6/2 mice by providing PLX3397 chow (275 ppm) from 6 to 11 weeks. They found that despite large microglia reductions, there were limited behavioural improvements in R6/2 carriers (Crapser, Ochaba et al. 2020). While they found that grip strength and cognition based on novel object recognition improved in carrier mice due to treatment, their performance on the rotarod and open field did not (Crapser, Ochaba et al. 2020). They also found that microglia

depletion did not improve striatal neuron survival based on $NeuN^+$ density but did reduce mhtt accumulation in R6/2 carriers (Crapser, Ochaba et al. 2020). Thus, taken together with our results, there is strong evidence that microglia in the symptomatic adult brain do not play a major role in the HD-related behaviours nor striatal neurodegeneration seen in R6/2 mice. Although this limits the therapeutic potential of microglia depletion in HD, the role of microglia in mhtt clearance and brain development still requires further research.

2.5.3 R6/2 carriers had a dampened response to PLX3397-induced microglia depletion

PLX3397 treatment at 600ppm resulted in large $Iba1^+$ microglia depletion in wildtype mice (91%; $p < 0.001$) which was greatly diminished in R6/2 carriers (57%; $p < 0.001$). The disparity between the genotypes was not due to the detection method. Iba1 – a macrophage- and microglia-specific calcium binding protein – was proven to appropriately identify microglia after PLX3397 treatment, as the remaining number of $Iba1^+$ microglia matched the number of GFP-tagged microglia in transgenic mice with GFP^+ myeloid lineage cells (Ohsawa, Imai et al. 2004, Elmore, Najafi et al. 2014). Furthermore, it is unlikely to be due to a difference in the amount of ingested PLX3397. The weight loss in R6/2 mice has been proven to be caused by increased metabolism and not a change in caloric intake (van der Burg, Bacos et al. 2008). Thus, the genotypic difference in $Iba1^+$ microglia suggests an innate resistance in R6/2 carriers to PLX3397-induced microglia depletion. This may be due to changes in the microglia themselves or ingested PLX3397 could be affected by their altered metabolism, such as altering its absorption into or clearance from the blood.

Furthermore, the extent of depletion for each microglia subtype differed between the genotypes. In R6/2 carriers, decreases were seen in the ramified (Low-dose: 60%; High-dose: 70%) and intermediate (Low-dose: 25%; High-dose: 56%) groups. In contrast, PLX3397 greatly affected all subtypes in wildtype littermates (78-92%). Additionally, PLX3397 treatment affected the subtype distribution of the remaining microglia, indicated by the relative increase in activated/amoeboid microglia in the PLX3397 groups compared to their vehicle counterparts (Fig. 7d). Elmore *et al.* (2014) also found that the remaining microglia had morphology reminiscent of activated microglia after PLX3397 treatment. Therefore, the mechanism of action for PLX3397 could be inducing microglia activation or be more selective for less activated

microglia. If the latter is true, the functional changes in microglia due to mhtt may have also altered their reactivity to PLX3397 in R6/2 carriers. Further research is required to elucidate if the resistance is metabolic or microglia-specific in nature.

2.5.4 Neuroimmune response may not play a major role in HD progression

Alterations in microglia appearance and functionality, such as hyperreactivity to inflammatory stimulus, have previously been reported in HD (Ma, Morton et al. 2003, Simmons, Casale et al. 2007, Crotti, Benner et al. 2014). In our study, R6/2 carriers showed higher baseline levels of microglia activation than their wildtype counterparts at 11.5 weeks based on their subtype prevalence. This supports the findings of increased microglia activation in HD (Schwab, Klegeris et al. 2010, Ellrichmann, Reick et al. 2013). However, the lack of physiological and behavioural improvements after microglia depletion indicates that hyperactive microglia do not play a significant role in the R6/2 model's HD symptomology after symptom onset (Crapser, Ochaba et al. 2020). Furthermore, increasing microglia activation using peripheral immune challenge had no effect on the motor coordination nor striatal volume in the YAC128 model (Franciosi, Ryu et al. 2012).

Conversely, changes in microglia functionality in R6/2 carriers are present from birth, with cell-autonomous pro-inflammatory transcriptional activation detected in primary microglia from newborn R6/2 mice (Crotti, Benner et al. 2014). At 3 weeks, increased phagocytosis, cellular stress, ferritin accumulation, and altered interactions with synapses have been detected in the R6/2 microglia (Simmons, Casale et al. 2007, Savage, St-Pierre et al. 2020). When Petkau *et al.* (2019) looked at the effect of mhtt in the BACHD mouse model of HD, they found that downregulating mhtt expression in microglia alone was able to reduce the auto-inflammatory aspects of microglia but was not sufficient to ameliorate the HD pathophysiology. Conversely, downregulating mhtt expression in neural progenitor cells – which mature into neurons, astrocytes, and oligodendrocytes – did not change $mhtt^{+}$ microglia hyperactivity but partially rescued some behavioural aspects of the HD model (Petkau, Hill et al. 2019). As downregulation of mhtt expression occurred from birth, this implies that $mhtt^{+}$ microglia's hyperactive response to inflammation does not have significant behavioural implications for HD during development. However, downregulating mhtt may not correct the other functional abnormalities present in

mhtt^{+} microglia, and the remaining presence of those abnormalities may impact HD outcome during brain development.

Furthermore, the R6/2 model lacks concrete evidence for upregulation of inflammatory factors. Some studies have reported that cytokine mRNA and protein levels in 10-12 week old R6/2 carriers are elevated in the striatum and in the plasma, while others have found no change in the striatum (Björkqvist, Wild et al. 2008, Godavarthi, Narender et al. 2009, Crotti, Benner et al. 2014, Crapser, Ochaba et al. 2020). This suggests that neuroinflammation may not play a prominent role in the R6/2 model's HD progression, which is surprising given the presence of inflammation in HD**.** While this does raise the question of how important neuroinflammation is for HD pathophysiology, this also raises the possibility that the lack of neuroinflammation may alter the role microglia has in the development of HD in the R6/2 model compared to HD patients.

The increased microglia activation seen in HD may be a result of other external factors, such as degenerating neurons, as even normal microglia become activated and proliferate in the presence of mhtt-expressing neurons *in vitro* (Kraft, Kaltenbach et al. 2012). Thus, the shift in microglia subtype prevalence in R6/2 carriers could be a result of microglia adapting to changes in the cellular environment elicited by HD pathology or mhtt-related functional changes in microglia, and not as a response to heightened inflammatory factors. Despite altered microglia functionality and increased microglia activation in HD, microglia do not appear to largely affect HD symptomology in symptomatic R6/2 carriers. Furthermore, limited evidence suggests that correcting microglia functionality in presymptomatic carriers does not benefit HD outcomes, but further research is required to confirm this result.

2.6 Conclusion

The elevated levels of microglia activation in seen in HD patients were also found in the R6/2 model. R6/2 carriers showed higher baseline levels of microglia activation than their wildtype littermates at 11.5 weeks, indicated by the shift in their distribution of microglia subtypes between vehicle groups. Although PLX3397 was able to reduce microglia in both genotypes, R6/2 carriers displayed a reduced ability to deplete microglia in response to PLX3397 (Low-dose: 31%, High-dose: 57%) compared to their wildtype littermates (High-dose: 91%). Further research is required to determine whether the reduced response is due to the $mhtt^{+}$ microglia responsiveness to PLX3397 or PLX3397 metabolism in the R6/2 model. Furthermore, there were signs of increased microglia activation after treatment which has also been seen by other groups. While R6/2 carriers and wildtype littermates in the vehicle groups followed the same behavioural patterns as those seen in the literature, microglia depletion from 6 weeks onwards did not ameliorate the HD symptoms in the carrier mice in both experiments, nor were there significant improvements in striatal neuron survival in the low-dose group. Based on this study, microglia do not have a large impact on the neuropathological nor behavioural symptoms in the R6/2 model after symptom onset.

Chapter 3: Perspectives on the Role of Microglia in Huntington's Disease Progression

3.1 Inflammation in HD

General inflammation is present in HD carriers, even prior to their motor symptom onset. Plasma levels of inflammatory cytokines increase over the course of the disease, with IL6 being the first detectable increase at 16 years prior to predicted symptom onset (Björkqvist, Wild et al. 2008). Initially, cytokines involved with the innate immune system (IL6, IL8) are heightened during the early stages of HD (Björkqvist, Wild et al. 2008). This is followed by cytokines involved with the adaptive immunity (IL10, IL4) as the disease state progresses, suggesting inflammation worsens over the disease course (Björkqvist, Wild et al. 2008). The cause for the increased inflammatory response in HD is likely from an innate source as the systemic humoral adaptive response to external pathogens is not activated, indicated by the stable immunoglobulin levels (IgG, IgA, IgM) throughout the disease progression (Björkqvist, Wild et al. 2008). These peripheral changes likely reflect systemic changes in the immune system in HD: IL6 and IL8 levels correlated between the CSF and plasma, and there is increased expression of inflammatory cytokines in the striatum and cortex (Björkqvist, Wild et al. 2008, Silvestroni, Faull et al. 2009).

Neuroinflammation is present in many neurodegenerative disorders other than HD, including AD, PD, and MS (Amor, Peferoen et al. 2014, Stephenson, Nutma et al. 2018). Whereas neuroinflammation in a healthy brain has been shown to help with recovery, neuroinflammation in neurodegenerative diseases appears to worsen the neurodegenerative damage (Amor, Peferoen et al. 2014, Gomez-Nicola and Perry 2015). Microglia are tightly regulated by the inflammatory response in the CNS (Amor, Peferoen et al. 2014). They normally play a role in maintaining homeostasis but have been found to be more activated in neurodegenerative diseases, possibly in response to the increased activation of the immune system (Gomez-Nicola and Perry 2015). In rodent models of AD, PD, and SCA, ablating microglia led to an improvement in some of their symptoms, further indicating a negative role of these abnormal perpetually active microglia (Spangenberg, Lee et al. 2016, Qu, Johnson et al. 2017, Sosna, Philipp et al. 2018, Oh, Ahn et al. 2020). Considering the similarities of increased

inflammation and microglia activation in HD and other neurodegenerative diseases, this led to our hypothesis that microglia may also play a detrimental role in HD progression.

3.2 Functionality of Wildtype and Mhtt-expressing Microglia

Microglia are involved with the normal development, function, and repair of the CNS. They constantly surveil their microenvironment, using their processes to look for changes (Gomez-Nicola and Perry 2015). They have a plethora of important roles for maintaining brain homeostasis during development and in adulthood, which include pruning synapses, phagocytosis of apoptotic debris and microbes, and inflammatory response (Gomez-Nicola and Perry 2015). In addition, they also use phagocytosis to prune synapses and clear toxic proteins (Gomez-Nicola and Perry 2015). Microglia may also play a role in determining functional brain connectivity and altering behaviour in the healthy brain during development, as the CX3CR1-CX3CL1 system involved with this is also believed to be used by microglia during synaptic pruning (Zhan, Paolicelli et al. 2014, Gomez-Nicola and Perry 2015).

Mhtt-expressing immune cells, including microglia, show functional changes in comparison to their wildtype counterparts. Monocytes from HD carriers, macrophages from the YAC128 model, and microglia from the R6/2 model have shown excessive cytokine response to sterile inflammation (Björkqvist, Wild et al. 2008). Their excessive response to inflammation may explain why there was pronouncedly increased neuronal death after LPS injection in the striatum of a mouse model with mhtt expression exclusively in their microglia (Crotti, Benner et al. 2014). $Mhtt^{+}$ microglia may also be contributing to the elevated inflammatory cytokine levels in HD, as both rodent and human $mhtt^{+}$ microglia have increased expression of pro-inflammatory factors (Crotti, Benner et al. 2014). Furthermore, microglia containing mhtt have shown reduced migration to chemotactic stimulus (Kwan, Träger et al. 2012). Their reliance on CSF1R signalling for survival may also be altered given that the R6/2 mice in our study were less responsive to microglia depletion through CSF1R inhibition (i.e. PLX3397) compared to their wildtype littermates. Although little is known about how the energy requirements for their highly motile processes are met, alterations in the mitochondria of MSNs are already heavily noted in the HD literature, and thus may also exist in microglia and impact their homeostatic role (Han, You et al. 2010, Gomez-Nicola and Perry 2015). Given the important roles of healthy microglia

both in development and adulthood, further research is still required to fully understand the extent of microglia's functional changes due to mhtt.

3.3 The Role of Microglia in HD progression

Microglia – the immune cells of the CNS – are key players in the neuroinflammatory response. They help reorganize adult circuitry following sensory loss or ischemia, and are suggested to also be involved with circuitry wiring during development (Wake, Moorhouse et al. 2009, Tremblay, Zettel et al. 2012, Gomez-Nicola and Perry 2015). While their phagocytotic role is beneficial in the healthy brain by removing debris before inflammation can occur, in brain pathologies with a neuroinflammatory element, microglia have been found to remove endangered-but-viable neurons as well (Brown and Neher 2014).

Microglia appear to reflect disease progression in HD. There are higher levels of activated microglia, especially in the striatum and cortex, in HD carriers prior to their motor symptom onset, which progressively grows in numbers as their disease state worsens (Tai, Pavese et al. 2007, Politis, Pavese et al. 2011, Politis, Lahiri et al. 2015). The level of microglia activation positively correlates with the 5-year probability of developing HD in presymptomatic carriers (Tai, Pavese et al. 2007). Furthermore, microglia density increases with increased neuronal loss (Sapp, Kegel et al. 2001, Tai, Pavese et al. 2007, Politis, Pavese et al. 2011). However, recent evidence in rodent models suggests that the functional abnormalities present in $mhtt^+$ microglia do not exacerbate the motor or behavioural symptoms of HD after symptom onset. Reducing mhtt expression in microglia alone restored their hyperactive response to sterile inflammation but did not improve the BACHD model's behavioural deficits for the open field test and the rotarod, nor prevented their striatal volume loss (Petkau, Hill et al. 2019). Systemic inflammation caused by chronic peripheral LPS injection led to increased microglia activation but did not impact motor coordination nor striatal volume loss in the YAC128 model of HD (Franciosi, Ryu et al. 2012). Furthermore, the results of our study and Crapser's study (2020) showed that depleting microglia in symptomatic R6/2 mice did not reduce striatal neurodegeneration nor improve many of their behavioural symptoms, except for reducing certain cognitive symptoms and mhtt accumulation. Thus, the functional changes and increased activation of $mhtt^+$ microglia don't appear to strongly affect the behavioural symptoms nor

striatal neurodegeneration in HD. Therefore, the increase in activated microglia may be as a response to the changing environment in HD. In addition to microglia's proinflammatory response to cell death, the progressive loss of neurons – which normally help downregulate the inflammatory pathway in microglia – may contribute to microglia's dysregulated proinflammatory state in HD (Gomez-Nicola and Perry 2015).

This is not to negate any role microglia may have on HD outcome during development. Changes in microglia functionality were noted in HD rodent models prior to symptom onset, which include increased phagocytosis, increased cellular stress, and altered interactions with synapses (Savage, St-Pierre et al. 2020). As the effects of $mhtt^{+}$ microglia's functional changes have not been fully explored, synaptic pruning and thus circuitry formation during brain development may be affected. Thus, $mhtt^{+}$ microglia may be involved in the impaired synaptic plasticity in cortical projection neurons and abnormal bidirectional connections between MSNs seen in HD (Blumenstock and Dudanova 2020). Therefore, although current rodent model evidence suggests that microglia do not have a role in HD pathogenesis after symptom onset, $mhtt^{+}$ microglia may still have an impact on HD outcome during the presymptomatic phase of their disease.

3.4 Strengths and Limitations

This study assessed the effects of microglia on the progressive behavioural and physiological changes in HD through pharmaceutical microglia ablation in the R6/2 mouse model. Experiments were performed at a dose commonly used in the literature (i.e. 290ppm) as well as at a higher dose for increased levels of microglia depletion. Both carrier and wildtype vehicle groups recapitulated the behavioural results of Samadi *et al.* (2013), and the lack of behavioural changes in wildtype mice after PLX3397-induced microglia depletion also matched the literature, except for the open field. Our results showed no indication that microglia depletion in treated R6/2 carriers results in behavioural improvements. Thus suggesting that microglia do not play a role in HD behavioural symptoms. The stereological estimates for the striatal microglia populations for R6/2 carriers and their wildtype littermates revealed that while the total number is lower in carrier mice, the microglia density is similar between the genotypes. This study also

revealed a lowered PLX3397 response in R6/2 carriers, but further research is required to discover the cause for their diminished response to PLX3397-induced microglia depletion.

There were a couple inherent limitations that came with the drug delivery method. Given the limited size of the cohorts, the level of microglia depletion over the course of the experiment could not be measured as it would have required sacrificing the mice. While there is the possibility of fluctuations in microglia numbers throughout the experiment, many sources in the literature have found that the majority of PLX3397-induced microglia depletion (70-90%) occurs within the first week and is maintained through continuous PLX3397 administration (Elmore, Najafi et al. 2014, Elmore, Lee et al. 2015). Furthermore, providing the PLX3397 chow *ad libitum* meant that the daily dose of ingested PLX3397 could not be regulated. This is an issue that exists in many PLX3397 studies. The quantity of PLX3397 ingested or in the brain should be addressed in future experiments, regardless of the animal model, to clarify the dose required for complete depletion and allow for better comparisons within the literature.

This study began supplying PLX3397 to the R6/2 mice at 6 weeks, which is after symptom onset in this HD model. However, functional changes in $mhtt^{+}$ microglia have been detected during the presymptomatic phase of HD (Simmons, Casale et al. 2007, Björkqvist, Wild et al. 2008). Therefore, it is plausible that microglia depletion after symptom onset is too late in the disease progression for notable behavioural improvements. Thus, this study does not address the role $mhtt^{+}$ microglia have during development, when the mice are presymptomatic, which may affect HD symptom progression and severity.

Finally, this study used the R6/2 mouse model to recapitulate HD. Although the R6/2 model mimics many neurological and physiological symptoms of HD, the genetic component of the R6/2 model is not representative of that naturally found in HD (Ramaswamy, McBride et al. 2007). Furthermore, the role of inflammation and the inflammatory system may differ between the R6/2 model and HD (Björkqvist, Wild et al. 2008, Godavarthi, Narender et al. 2009, Crotti, Benner et al. 2014, Crapser, Ochaba et al. 2020). Therefore, although rodent model evidence suggests microglia do not have a prominent role in the HD symptom outcome after symptom onset, their role in the human pathology may be different.

3.5 Future Applications

Although microglia depletion in the R6/2 model showed no behavioural improvements, further assessment of the cellular changes is still required to fully understand microglia's role in HD pathogenesis. Striatal neurodegeneration of $Nissl^+$ cells was unaffected by low-dose treatment, but there was a trend for increased parvalbumin (PV) interneuron survival in the treated group. Stereology of $Nissl^+$ neurons and PV interneurons in the High-dose group could elucidate whether neurodegeneration is altered by more substantial microglia depletion. Furthermore, future experiments could compare cytokine levels in the brain between treatment groups to better understand the impact microglia has on neuroinflammation in HD and between genotypes to clarify whether there is increased neuroinflammation in the R6/2 model.

R6/2 carriers had reduced PLX3397-induced microglia depletion compared to their wildtype littermates, implying that the R6/2 model is more resistant to microglia depletion through CSF1R inhibition. This increased resistance to CSF1R inhibition could be from another mhtt-related change in microglia functionality. An *in vitro* study could elucidate if the resistance is an innate characteristic of $mhtt^+$ microglia through comparing their responsiveness to a fixed dose of PLX3397 to wildtype microglia. Further research could also look if the receptors targeted by PLX3397 – CSF1R, cKIT, FLT3 – are downregulated or otherwise altered in microglia in HD. It is also plausible that the reduced responsiveness of R6/2 mice to PLX3397 is the result of altered drug absorption, distribution, metabolism, or excretion in HD. Increased metabolism has already been noted in the R6/2 model (van der Burg, Bacos et al. 2008). Future *in vivo* experiments in R6/2 mice should use a fixed daily dosage and quantify PLX3397 levels in the brain to check for HD-related changes in PLX3397 metabolism.

When comparing the relative abundance of microglia subtypes between treatment groups, the extent of microglia depletion decreased with increased microglia activation for both genotypes. However, after treatment, carriers had proportionally less depletion for more activated microglia subtypes than wildtype littermates. This suggests activated $mhtt^+$ microglia may have greater resistance to PLX3397 compared to activated wildtype microglia. Alternatively, $mhtt^+$ microglia could be more primed for activation due to their functional abnormalities, and activation of the remaining microglia was triggered as a response to the PLX3397-induced apoptosis occurring in their environment. Further research is required to

determine if and why PLX3397-induced depletion is less effective in activated microglia, especially in microglia containing mhtt.

Hyperactive microglia may still play a detrimental role on HD outcome during brain development and maturation. Altered microglia functionality is reported from birth and throughout the presymptomatic phase in the R6/2 model, which is well before our experiment starting point of 6 weeks (Simmons, Casale et al. 2007, Crotti, Benner et al. 2014, Savage, St-Pierre et al. 2020). Although Petkau *et al.* (2019) showed that correcting the hyperactivity of $mhtt^+$ microglia did not improve the behavioural nor neuropathological aspects of HD in the BACHD model, $mhtt^+$ microglia's other functional abnormalities could have still impacted HD outcome as they were not tested for and could still be present after downregulating mhtt. In summary, while the functional abnormalities of $mhtt^+$ microglia and increased microglia activation in HD were not found to have significant behavioural implications in symptomatic HD carriers, the impact of $mhtt^+$ microglia on the developing brain on HD outcome requires further research.

Appendix

A1 Experimental Timeline

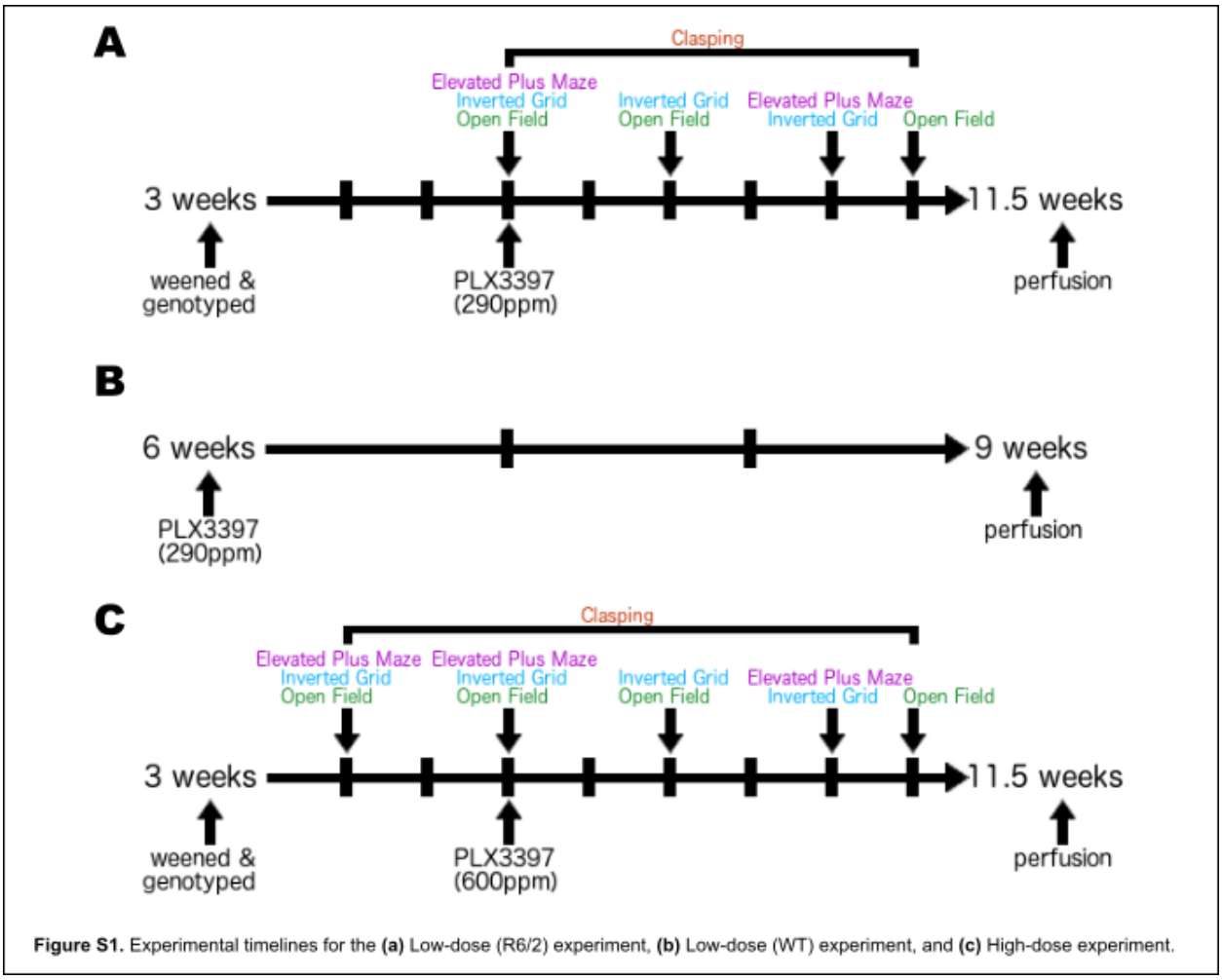

Figure S1. Experimental timelines for the **(a)** Low-dose (R6/2) experiment, **(b)** Low-dose (WT) experiment, and **(c)** High-dose experiment.

A2 Supplementary Figures

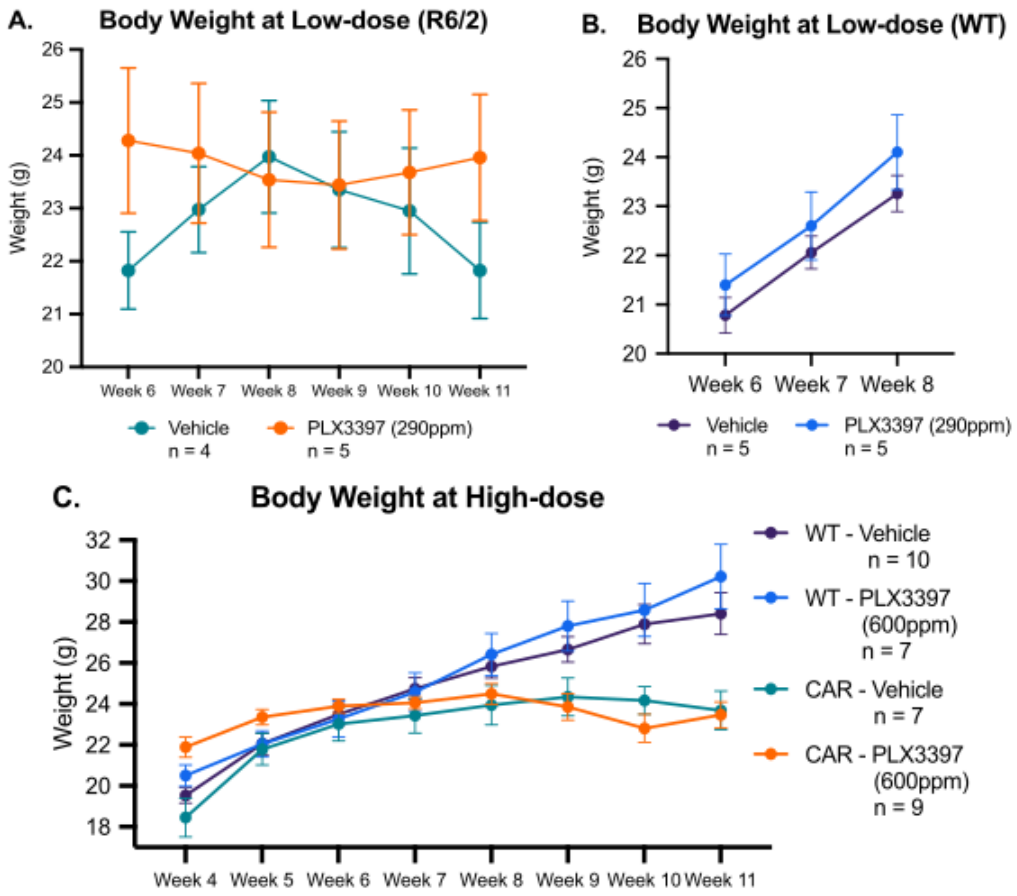

Figure S2. The body weight increased with age for both wildtype groups, but fluctuated over time between the R6/2 carrier groups – likely due to their large variability in weight prior to PLX3397 treatment (i.e. weeks 4-6). **(a)** While there was a significant interactive effect between age and treatment in R6/2 carriers from the Low-dose (R6/2) experiment ($F(5, 35) = 4.94$, $p = 0.002$, partial $\eta 2 = 0.414$), posthoc tests showed no significant weight differences at any of the timepoints (6w $p = 0.188$, 7w $p = 0.541$, 8w $p = 0.808$, 9w $p = 0.959$, 10w $p = 0.680$, 11w $p = 0.216$). **(b)** Wildtype mice in the Low-dose (WT) experiment showed no difference in weight gain over time between the treatment groups ($F(2,16) = 0.20$, $p = 0.824$, partial $\eta 2 = 0.024$), which increased for both groups with age ($F(2,16) = 54.44$, $p < 0.001$), and both treatment groups had similar weight averages ($F(1,8) = 0.84$, $p = 0.385$). **(c)** Changes in body weight over time in the High-dose experiment were dependent on both treatment group and genotype ($F(7) = 4.37$, $p < 0.001$). Between vehicle groups, carrier mice began to plateau around 7 weeks while wildtype mice continued to gain weight ($F(7) = 8.39$, $p < 0.001$), however posthoc tests revealed no timepoints of significance (4w $p = 0.888$, 5w-6w $p = 1.000$, 7w $p = 0.888$, 8w $p = 0.712$, 9w $p = 0.241$, 10w $p = 0.196$, 11w $p = 0.153$). Wildtype mice showed no interaction between treatment and age ($F(7) = 1.32$, $p = 0.246$), had similar average weights between treatment groups ($F(1) = 0.21$, $p = 0.650$), and increased in weight over time in both treatment groups ($F(7) = 121.84$, $p < 0.001$). There were significant weight variations between the carrier treatment groups over time ($F(7) = 6.41$, $p < 0.001$), however all timepoints were non-significant (4w $p = 0.092$, 5w $p = 0.498$, 6w-9w $p = 1.000$, 10w $p = 0.828$, 11w $p = 1.000$).

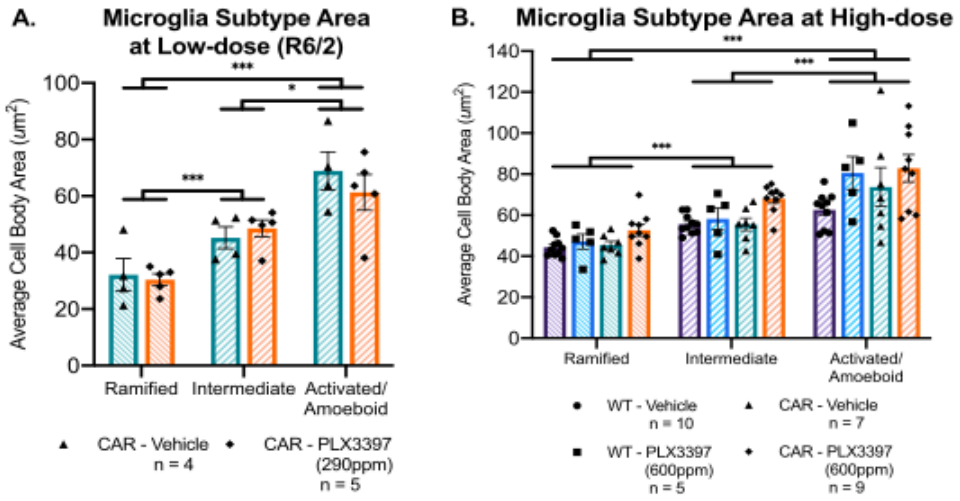

Figure S3. The average cell body area for each microglia subtype was consistent across all genotype and treatment groups. The area of the soma significantly differed between all microglia subtypes in both **(a)** the Low-dose (R6/2) experiment (Greenhouse-Geisser correction: $F(1.132, 7.925) = 31.27$, $p < 0.001$, partial $\eta 2 = 0.817$) and **(b)** the High-dose experiment (Greenhouse-Geisser correction: $F(1.367, 36.904) = 43.04$, $p < 0.001$, partial $\eta 2 = 0.614$). In the High-dose experiment, the collective average cell body area was larger in the treated groups compared to the untreated groups ($F(1, 27) = 9.37$, $p = 0.005$, partial $\eta 2 = 0.258$), which indicates that PLX3397 was causing the microglia soma to increase. This may indicate that the remaining microglia are more primed for activation after treatment. Two wildtype mice from the treated group had to be excluded from the High-dose analysis due to the lack of samples for all subtypes.

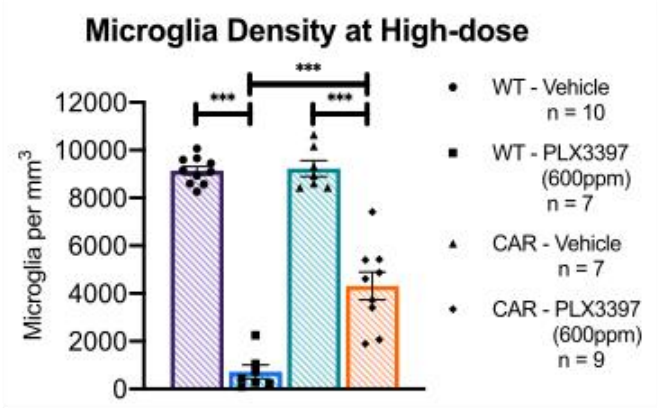

Figure S4. PLX3397-induced microglia depletion led to a differential response between the genotypes in the High-dose experiment based on their microglia densities in the striatum ($F(1) = 22.48$, $p < 0.001$). There was no difference in density between the vehicle groups ($p = 0.962$), and PLX3397 treatment was effective in reducing microglia for both genotypes (WT: $p < 0.001$; CAR: $p < 0.001$). However, microglia density was significantly higher in the treated carrier group compared to the treated wildtype group ($p < 0.001$), indicating a difference between the genotypes in their responsiveness to PLX3397-induced microglia depletion.

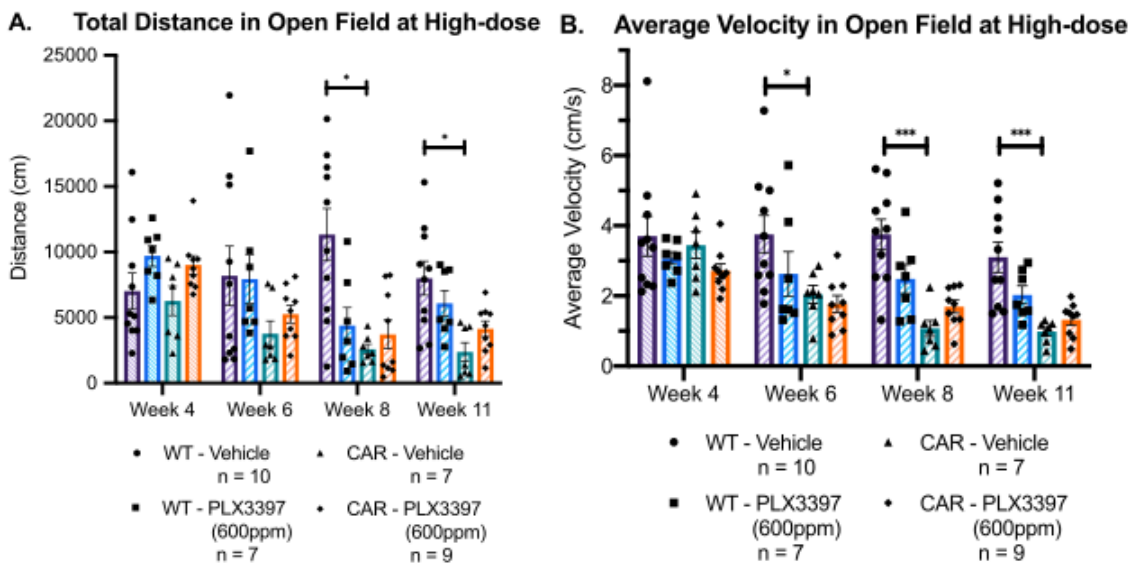

Figure S5. While the open field test revealed the expected genotypic pattern between vehicle groups, PLX3397 treatment was not beneficial to, and may have worsened, their performance. **(a)** The pattern for the total distance travelled in the open field was dependent on treatment group, genotype, and age ($F(3) = 3.71$, $p = 0.015$). Between the untreated groups, R6/2 carriers travelled less distance than wildtype controls over time ($F(3) = 5.24$, $p = 0.003$), with significant differences starting from 8 weeks (4w $p = 0.845$, 6w $p = 0.540$, 8w $p = 0.014$, 11w $p = 0.012$). For wildtype mice, the treated group performed progressively worse than the control group ($F(3) = 6.03$, $p = 0.002$), but posthoc tests found no significant differences at any of the timepoints (w4 $p = 0.263$, w6 $p = 0.630$, w8 $p = 0.100$, w11 $p = 0.630$). There was no interaction between treatment and age in the R6/2 carriers ($F(3) = 0.44$, $p = 0.727$). The treated carriers travelled further than the untreated carriers on average ($F(1) = 5.91$, $p = 0.029$), but both groups declined with age ($F(3) = 16.79$, $p < 0.001$). **(b)** Changes in average velocity were also dependent on treatment group, genotype, and age ($F(3) = 2.80$, $p = 0.045$). Vehicle R6/2 carriers progressively performed worse than their wildtype counterparts ($F(3) = 4.07$, $p = 0.012$), with significant differences starting from 6 weeks (w4 $p = 1.000$, w6 $p = 0.050$, w8 and w11 $p < 0.001$) . In wildtype mice, treatment did not alter their average velocity over time ($F(3) = 0.72$, $p = 0.548$) nor did their average velocity change with age ($F(3) = 1.08$, $p = 0.367$), but the treated group did have a lower average velocity than the vehicle group overall ($F(1) = 5.86$, $p = 0.029$). While the pattern of average velocity over time was different between carrier treatment groups ($F(3) = 4.04$, $p = 0.013$), there were no specific timepoints of significance (w4 $p = 0.348$, w6 $p = 0.536$, w8 $p = 0.124$, w11 $p = 0.342$).

Bibliography

Achkova, D. and J. Maher (2016). "Role of the colony-stimulating factor (CSF)/CSF-1 receptor axis in cancer." Biochem Soc Trans **44**(2): 333-341.

Amor, S., et al. (2014). "Inflammation in neurodegenerative diseases--an update." Immunology **142**(2): 151-166.

Báez-Mendoza, R. and W. Schultz (2013). "The role of the striatum in social behavior." Front Neurosci **7**: 233.

Barres, B., et al. (2015). Glia, Cold Spring Harbor Laboratory Press.

Bennett, R. E., et al. (2018). "Partial reduction of microglia does not affect tau pathology in aged mice." Journal of neuroinflammation **15**(1): 311.

Bilimoria, P. M. and B. Stevens (2015). "Microglia function during brain development: new insights from animal models." Brain Research **1617**: 7-17.

Björkqvist, M., et al. (2008). "A novel pathogenic pathway of immune activation detectable before clinical onset in Huntington's disease." Journal of Experimental Medicine **205**(8): 1869-1877.

Blumenstock, S. and I. Dudanova (2020). "Cortical and Striatal Circuits in Huntington's Disease." Front Neurosci **14**: 82.

Brown, G. C. and J. J. Neher (2014). "Microglial phagocytosis of live neurons." Nature Reviews Neuroscience **15**(4): 209.

Capsoni, S., et al. (2012). "Pathogen free conditions slow the onset of neurodegeneration in a mouse model of nerve growth factor deprivation." J Alzheimers Dis **31**(1): 1-6.

Cowin, R.-M., et al. (2011). "Onset and progression of behavioral and molecular phenotypes in a novel congenic R6/2 line exhibiting intergenerational CAG repeat stability." PLoS One **6**(12): e28409.

Crapser, J. D., et al. (2020). "Microglial depletion prevents extracellular matrix changes and striatal volume reduction in a model of Huntington's disease." Brain **143**(1): 266-288.

Crevier-Sorbo, G., et al. (2020). "Thalamostriatal degeneration contributes to dystonia and cholinergic interneuron dysfunction in a mouse model of Huntington’s disease." Acta Neuropathologica Communications **8**(1): 14.

Crotti, A., et al. (2014). "Mutant Huntingtin promotes autonomous microglia activation via myeloid lineage-determining factors." Nature Neuroscience **17**(4): 513.

da Fonseca, A. C. C., et al. (2014). "The impact of microglial activation on blood-brain barrier in brain diseases." Frontiers in cellular neuroscience **8**: 362.

Daiichi Sankyo, I. (2015). "Phase 3 Study of Pexidartinib for Pigmented Villonodular Synovitis (PVNS) or Giant Cell Tumor of the Tendon Sheath (GCT-TS) (ENLIVEN)."

Davies, S. W., et al. (1997). "Formation of Neuronal Intranuclear Inclusions Underlies the Neurological Dysfunction in Mice Transgenic for the HD Mutation." Cell **90**(3): 537-548.

Deacon, R. M. J. (2013). "Measuring the strength of mice." Journal of visualized experiments: JoVE(76).

DeBoy, C. A., et al. (2010). "FLT-3 expression and function on microglia in multiple sclerosis." Experimental and molecular pathology **89**(2): 109-116.

Dodds, L., et al. (2014). "Characterization of striatal neuronal loss and atrophy in the R6/2 mouse model of Huntington's disease." PLoS currents **6**.

El-Gamal, M. I., et al. (2018). "Recent advances of colony-stimulating factor-1 receptor (CSF-1R) kinase and its inhibitors." Journal of medicinal chemistry **61**(13): 5450-5466.

Ellrichmann, G., et al. (2013). "The role of the immune system in Huntington's disease." Clinical and Developmental Immunology **2013**.

Elmore, M. R. P., et al. (2015). "Characterizing newly repopulated microglia in the adult mouse: impacts on animal behavior, cell morphology, and neuroinflammation." PLoS One **10**(4): e0122912.

Elmore, M. R. P., et al. (2014). "CSF1 receptor signaling is necessary for microglia viability, which unmasks a cell that rapidly repopulates the microglia-depleted adult brain." Neuron **82**(2): 380.

Ferrante, R. J. (2009). "Mouse models of Huntington's disease and methodological considerations for therapeutic trials." Biochimica et Biophysica Acta (BBA)-Molecular Basis of Disease **1792**(6): 506-520.

File, S. E., et al. (1998). "Striking changes in anxiety in Huntington's disease transgenic mice." Brain Research **805**(1): 234-240.

Franciosi, S., et al. (2012). "Age-dependent neurovascular abnormalities and altered microglial morphology in the YAC128 mouse model of Huntington disease." Neurobiol Dis **45**(1): 438-449.

Godavarthi, S. K., et al. (2009). "Induction of chemokines, MCP-1, and KC in the mutant huntingtin expressing neuronal cells because of proteasomal dysfunction." Journal of Neurochemistry **108**(3): 787-795.

Gomez-Nicola, D. and V. H. Perry (2015). "Microglial dynamics and role in the healthy and diseased brain: a paradigm of functional plasticity." The Neuroscientist : a review journal bringing neurobiology, neurology and psychiatry **21**(2): 169-184.

Guo, Z., et al. (2012). "Striatal neuronal loss correlates with clinical motor impairment in Huntington's disease." Movement Disorders **27**(11): 1379-1386.

Guyenet, S. J., et al. (2010). "A simple composite phenotype scoring system for evaluating mouse models of cerebellar ataxia." Journal of visualized experiments: JoVE(39).

Han, I., et al. (2010). "Differential vulnerability of neurons in Huntington's disease: the role of cell type-specific features." Journal of Neurochemistry **113**(5): 1073-1091.

Harris, R. A. and S. Amor (2011). "Sweet and sour--oxidative and carbonyl stress in neurological disorders." CNS Neurol Disord Drug Targets **10**(1): 82-107.

Hashimoto, D., et al. (2013). "Tissue-resident macrophages self-maintain locally throughout adult life with minimal contribution from circulating monocytes." Immunity **38**(4): 792-804.

Hsiao, H.-Y., et al. (2014). "Inhibition of soluble tumor necrosis factor is therapeutic in Huntington's disease." Human Molecular Genetics **23**(16): 4328-4344.

Huang, Y., et al. (2018). "Repopulated microglia are solely derived from the proliferation of residual microglia after acute depletion." Nature Neuroscience **21**(4): 530-540.

Imarisio, S., et al. (2008). "Huntington's disease: from pathology and genetics to potential therapies." Biochemical Journal **412**(2): 191-209.

Jaturapatporn, D., et al. (2012). "Aspirin, steroidal and non-steroidal anti-inflammatory drugs for the treatment of Alzheimer's disease." Cochrane Database of Systematic Reviews(2).

Kawabori, M. and M. A. Yenari (2015). "The role of the microglia in acute CNS injury." Metabolic brain disease **30**(2): 381-392.

Komada, M., et al. (2008). "Elevated plus maze for mice." Journal of visualized experiments: JoVE(22).

Kraft, A. D., et al. (2012). "Activated microglia proliferate at neurites of mutant huntingtin-expressing neurons." Neurobiology of aging **33**(3): 621.e617-621.e626.621E633.

Kwan, W., et al. (2012). "Mutant huntingtin impairs immune cell migration in Huntington disease." The Journal of clinical investigation **122**(12): 4737-4747.

Li, C., et al. (2013). "Impact of minocycline on neurodegenerative diseases in rodents: a meta-analysis." Rev Neurosci **24**(5): 553-562.

Li, H.-D., et al. (2017). "A translocator protein 18 kDa agonist protects against cerebral ischemia/reperfusion injury." Journal of neuroinflammation **14**(1): 151.

Li, J. Y., et al. (2005). "The use of the R6 transgenic mouse models of Huntington's disease in attempts to develop novel therapeutic strategies." NeuroRx **2**(3): 447-464.

Li, M., et al. (2017). "Colony stimulating factor 1 receptor inhibition eliminates microglia and attenuates brain injury after intracerebral hemorrhage." Journal of Cerebral Blood Flow & Metabolism **37**(7): 2383-2395.

Li, Q. and B. A. Barres (2018). "Microglia and macrophages in brain homeostasis and disease." Nat Rev Immunol **18**(4): 225-242.

Li, S.-H. and X.-J. Li (2004). "Huntingtin–protein interactions and the pathogenesis of Huntington's disease." TRENDS in Genetics **20**(3): 146-154.

Lull, M. E. and M. L. Block (2010). "Microglial activation and chronic neurodegeneration." Neurotherapeutics **7**(4): 354-365.

Ma, L., et al. (2003). "Microglia density decreases with age in a mouse model of Huntington's disease." Glia **43**(3): 274-280.

Mangiarini, L., et al. (1996). "Exon 1 of the HD gene with an expanded CAG repeat is sufficient to cause a progressive neurological phenotype in transgenic mice." Cell **87**(3): 493-506.

Masnata, M., et al. (2019). "Demonstration of prion-like properties of mutant huntingtin fibrils in both in vitro and in vivo paradigms." Acta Neuropathol **137**(6): 981-1001.

Mok, S., et al. (2014). "Inhibition of CSF-1 receptor improves the antitumor efficacy of adoptive cell transfer immunotherapy." Cancer research **74**(1): 153-161.

Morigaki, R. and S. Goto (2017). "Striatal vulnerability in Huntington's disease: Neuroprotection versus neurotoxicity." Brain sciences **7**(6): 63.

Morsali, D., et al. (2013). "Safinamide and flecainide protect axons and reduce microglial activation in models of multiple sclerosis." Brain **136**(Pt 4): 1067-1082.

Myers, R. H., et al. (1991). "Decreased neuronal and increased oligodendroglial densities in Huntington's disease caudate nucleus." Journal of Neuropathology & Experimental Neurology **50**(6): 729-742.

Nayak, A., et al. (2011). "Huntington's disease: an immune perspective." Neurology research international **2011**.

Nimmerjahn, A., et al. (2005). "Resting microglial cells are highly dynamic surveillants of brain parenchyma in vivo." Science **308**(5726): 1314-1318.

Oh, S. J., et al. (2020). "Evaluation of the Neuroprotective Effect of Microglial Depletion by CSF-1R Inhibition in a Parkinson's Animal Model." Molecular Imaging and Biology.

Ohsawa, K., et al. (2004). "Microglia/macrophage-specific protein Iba1 binds to fimbrin and enhances its actin-bundling activity." Journal of Neurochemistry **88**(4): 844-856.

Paldino, E., et al. (2017). "Selective Sparing of Striatal Interneurons after Poly (ADP-Ribose) Polymerase 1 Inhibition in the R6/2 Mouse Model of Huntington's Disease." Frontiers in neuroanatomy **11**: 61.

Pavese, N., et al. (2006). "Microglial activation correlates with severity in Huntington disease: a clinical and PET study." Neurology **66**(11): 1638-1643.

Paxinos, G. and K. B. J. Franklin (2004). The mouse brain in stereotaxic coordinates, Gulf professional publishing.

Perdiguero, E. G., et al. (2015). "Tissue-resident macrophages originate from yolk-sac-derived erythro-myeloid progenitors." Nature **518**(7540): 547.

Perry, V. H. (2010). "Contribution of systemic inflammation to chronic neurodegeneration." Acta Neuropathologica **120**(3): 277-286.

Petkau, T. L., et al. (2019). "Mutant huntingtin expression in microglia is neither required nor sufficient to cause the Huntington's disease-like phenotype in BACHD mice." Human Molecular Genetics **28**(10): 1661-1670.

Politis, M., et al. (2015). "Increased central microglial activation associated with peripheral cytokine levels in premanifest Huntington's disease gene carriers." Neurobiology of disease **83**: 115-121.

Politis, M., et al. (2011). "Microglial activation in regions related to cognitive function predicts disease onset in Huntington's disease: a multimodal imaging study." Hum Brain Mapp **32**(2): 258-270.

Qu, W., et al. (2017). "Inhibition of colony-stimulating factor 1 receptor early in disease ameliorates motor deficits in SCA1 mice." Journal of neuroinflammation **14**(1): 107.

Ramaswamy, S., et al. (2007). "Animal models of Huntington's disease." Ilar j **48**(4): 356-373.

Reiner, A., et al. (2013). "Striatal parvalbuminergic neurons are lost in Huntington's disease: implications for dystonia." Movement Disorders **28**(12): 1691-1699.

Réu, P., et al. (2017). "The lifespan and turnover of microglia in the human brain." Cell reports **20**(4): 779-784.

Rice, R. A., et al. (2015). "Elimination of microglia improves functional outcomes following extensive neuronal loss in the hippocampus." Journal of Neuroscience **35**(27): 9977-9989.

Roos, R. A. C. (2010). "Huntington's disease: a clinical review." Orphanet journal of rare diseases **5**(1): 40.

Roze, E., et al. (2011). "Huntington's disease and striatal signaling." Frontiers in neuroanatomy **5**: 55.

Sadikot, A. F. and R. Sasseville (1997). "Neurogenesis in the mammalian neostriatum and nucleus accumbens: parvalbumin-immunoreactive GABAergic interneurons." J Comp Neurol **389**(2): 193-211.

Samadi, P., et al. (2013). "Relationship between BDNF expression in major striatal afferents, striatum morphology and motor behavior in the R6/2 mouse model of Huntington's disease." Genes, Brain and Behavior **12**(1): 108-124.

Sapp, E., et al. (2001). "Early and progressive accumulation of reactive microglia in the Huntington disease brain." Journal of Neuropathology & Experimental Neurology **60**(2): 161-172.

Sari, Y. (2011). "Huntington's Disease: From Mutant Huntingtin Protein to Neurotrophic Factor Therapy." Int J Biomed Sci **7**(2): 89-100.

Sathasivam, K., et al. (1999). "Formation of Polyglutamine Inclusions in Non-CNS Tissue." Human Molecular Genetics **8**(5): 813-822.

Saudou, F., et al. (1998). "Huntingtin acts in the nucleus to induce apoptosis but death does not correlate with the formation of intranuclear inclusions." Cell **95**(1): 55-66.

Savage, J. C., et al. (2020). "Microglial physiological properties and interactions with synapses are altered at presymptomatic stages in a mouse model of Huntington's disease pathology." Journal of neuroinflammation **17**(1): 98.

Sawa, A., et al. (2003). "Mechanisms of neuronal cell death in Huntington's disease." Cytogenet Genome Res **100**(1-4): 287-295.

Sawa, A., et al. (1999). "Increased apoptosis of Huntington disease lymphoblasts associated with repeat length-dependent mitochondrial depolarization." Nat Med **5**(10): 1194-1198.

Schwab, C., et al. (2010). "Inflammation in transgenic mouse models of neurodegenerative disorders." Biochimica et Biophysica Acta (BBA)-Molecular Basis of Disease **1802**(10): 889-902.

Shimada, A. and S. Hasegawa-Ishii (2011). "Senescence-accelerated Mice (SAMs) as a Model for Brain Aging and Immunosenescence." Aging Dis **2**(5): 414-435.

Silvestroni, A., et al. (2009). "Distinct neuroinflammatory profile in post-mortem human Huntington's disease." Neuroreport **20**(12): 1098-1103.

Simmons, D. A., et al. (2007). "Ferritin accumulation in dystrophic microglia is an early event in the development of Huntington's disease." Glia **55**(10): 1074-1084.

Sosna, J., et al. (2018). "Early long-term administration of the CSF1R inhibitor PLX3397 ablates microglia and reduces accumulation of intraneuronal amyloid, neuritic plaque deposition and pre-fibrillar oligomers in 5XFAD mouse model of Alzheimer's disease." Molecular neurodegeneration **13**(1): 11.

Spangenberg, E. E., et al. (2016). "Eliminating microglia in Alzheimer's mice prevents neuronal loss without modulating amyloid-β pathology." Brain **139**(4): 1265-1281.

Stephenson, J., et al. (2018). "Inflammation in CNS neurodegenerative diseases." Immunology **154**(2): 204-219.

Tai, Y. F., et al. (2007). "Imaging microglial activation in Huntington's disease." Brain Res Bull **72**(2-3): 148-151.

Tap, W. D., et al. (2015). "Structure-Guided Blockade of CSF1R Kinase in Tenosynovial Giant-Cell Tumor." N Engl J Med **373**(5): 428-437.

Tatem, K. S., et al. (2014). "Behavioral and locomotor measurements using an open field activity monitoring system for skeletal muscle diseases." Journal of visualized experiments: JoVE(91).

Torres-Platas, S. G., et al. (2014). "Morphometric characterization of microglial phenotypes in human cerebral cortex." Journal of neuroinflammation **11**: 12-12.

Tremblay, M.-È., et al. (2012). "Effects of aging and sensory loss on glial cells in mouse visual and auditory cortices." Glia **60**(4): 541-558.

van der Burg, J. M. M., et al. (2008). "Increased metabolism in the R6/2 mouse model of Huntington's disease." Neurobiology of disease **29**(1): 41-51.

Wake, H., et al. (2009). "Resting microglia directly monitor the functional state of synapses in vivo and determine the fate of ischemic terminals." The Journal of neuroscience : the official journal of the Society for Neuroscience **29**(13): 3974-3980.

Walf, A. A. and C. A. Frye (2007). "The use of the elevated plus maze as an assay of anxiety-related behavior in rodents." Nature protocols **2**(2): 322.

Webster, C. M., et al. (2013). "Microglial P2Y12 deficiency/inhibition protects against brain ischemia." PLoS One **8**(8): e70927.

Wobbrock, J. O., et al. (2011). The aligned rank transform for nonparametric factorial analyses using only anova procedures. Proceedings of the SIGCHI Conference on Human Factors in Computing Systems. Vancouver, BC, Canada, Association for Computing Machinery**:** 143–146.

Yang, H.-M., et al. (2017). "Microglial activation in the pathogenesis of Huntington's disease." Frontiers in aging neuroscience **9**: 193.

Zhan, Y., et al. (2014). "Deficient neuron-microglia signaling results in impaired functional brain connectivity and social behavior." Nat Neurosci **17**(3): 400-406.

Zhang, S.-C. and S. Fedoroff (1997). "Cellular localization of stem cell factor and c-kit receptor in the mouse nervous system." Journal of neuroscience research **47**(1): 1-15.

Zhang, S.-C. and S. Fedoroff (1998). "Modulation of microglia by stem cell factor." Journal of neuroscience research **53**(1): 29-37.

Zhang, S.-C. and S. Fedoroff (1999). "Expression of stem cell factor and c-kit receptor in neural cells after brain injury." Acta Neuropathologica **97**(4): 393-398.

Zuccato, C. and E. Cattaneo (2007). "Role of brain-derived neurotrophic factor in Huntington's disease." Progress in neurobiology **81**(5-6): 294-330.